doi: 10.82124/CEAS-GNC-2026-069 CEAS-GNC-2026-069

Robust Model Predictive Control for Rendezvous with Relative Orbital Elements and System Level Synthesis

Afonso Botelho PhD Candidate, Instituto Superior Técnico, Universidade de Lisboa, INESC-ID, and DEIMOS Engenharia, Lisbon, Portugal. afonso.botelho@tecnico.ulisboa.pt

Paulo Rosa Head of Flight Segment, DEIMOS Engenharia, Lisbon, Portugal. parosa@indracompany.com

João M. Lemos Full Professor, Instituto Superior Técnico, Universidade de Lisboa, Lisbon, Portugal
Senior Researcher, INESC-ID, Lisbon, Portugal. jlml@inesc-id.pt

ABSTRACT

We propose a System Level Synthesis (SLS) Model Predictive Control (MPC) approach to guidance and control (G&C) of the relative orbit for spacecraft rendezvous. SLS-MPC jointly optimizes a nominal trajectory and linear correction policy via convex optimization, which provides improved performance and feasibility with respect to practical Robust MPC (RMPC) methods, namely Linear Tube-Based MPC, which solely optimizes the nominal trajectory. Although this improvement comes at the cost of increased computational complexity, we show that a single initial SLS optimization can generate a nominal trajectory and correction policy that achieves performance comparable to standard RMPC, in a strategy which we call *One-Shot* SLS-MPC. Therefore, SLS can soften the dependence of MPC on real-time and recursive optimization, and more so given that the sole crucial optimization problem may be solved prior to the manoeuvre start while maintaining a time-flexible and safe hold point. Alternative deployment strategies are also discussed, which allow for trading-off between G&C performance and computational complexity. We also leverage a relative orbital element (ROE) state representation, in particular to formulate a novel simple and convex passive safety path constraint with limited conservativeness, and a dynamical prediction model that includes both J_2 and drag perturbations. Numerical results in a far-range rendezvous scenario show the improved fuel performance and feasibility of SLS-MPC with respect to Linear Tube-Based MPC.

Keywords: Model Predictive Control (MPC), System Level Synthesis (SLS), Onboard Optimization, Rendezvous and Proximity Operations (RPO), Guidance and Control (G&C)

1 Introduction

Model Predictive Control (MPC) [1] has been extensively researched in application to spacecraft guidance and control (G&C) for orbital rendezvous [2–8], promising potential improvements in performance, fuel efficiency, safety, and autonomy with respect to classical methods. Real-flight experiments have been reported, e.g., for the PRISMA in-orbit test bed [9], but are scarce, and the use of classical G&C methods, i.e., linear controllers and analytical guidance laws [10], is still the standard industrial practice. This is mainly due to the reliance of MPC on real-time and recursive numerical optimization, which has a significant algorithmic and computational complexity compared to classical methods and

with respect to the limited computational power available for a typical onboard computer (OBC). Furthermore, optimization solvers often lack bounded execution time guarantees, and thus the MPC cannot be guaranteed to always provide a feasible control decision within the available timeslot, which may be incompatible with the safety-critical requirements intrinsic to these missions. On the other hand, designing a computationally efficient Robust MPC (RMPC) with performance and safety guarantees for all relevant dynamic effects, disturbances, and uncertainties without excessive conservatism also remains a challenge. Moreover, given that MPC is a nonlinear control method, any such guarantees differ in nature from those available for classical methods, e.g., frequency and linear stability analysis [10], which further deters its adoption in industrial practice. Nonetheless, the emerging Commercial Space paradigm [11] and onset of novel rendezvous and proximity operations (RPO) applications, namely autonomous in-orbit servicing (IOS), active debris removal (ADR), and cislunar RPO, motivate the research and development of advanced G&C methods to enable such missions or at least improve their performance, fuel efficiency, safety, and autonomy.

We propose a RMPC based on finite-horizon System Level Synthesis (SLS) for performing closed-loop guidance and control of the relative orbit for rendezvous while considering control limitations, passive safety requirements, and manoeuvre accuracy requirements, while minimizing a robust fuel-consumption metric. SLS is a control synthesis framework for linear systems and linear time-varying (LTV) state-feedback controllers that leverages a special parameterization of the disturbed closed-loop system response that enables an exact convex re-formulation of the controller synthesis problem [12]. This relatively recent parameterization is equivalent [13] to the well-known and established Youla parameterization [14], but is better suited for state-feedback control synthesis and imposing time-domain state and control constraints. Therefore, it is combinable with the MPC framework to design a RMPC state-feedback policy online simultaneously with a nominal trajectory while retaining a convex optimization problem [15, 16]. In comparison, practical Tube-Based MPC methods may also consider a linear feedback controller [1], known as the *ancillary* controller, which is used to provide conservative bounds for the disturbed closed-loop state — known as *tubes* or reachable sets — about the optimized nominal trajectory, which are then used to tighten the MPC constraints to ensure robust constraint satisfaction and recursive feasibility. However, to enable a convex and computationally efficient optimization, the ancillary is typically determined offline and fixed during online use [1]. SLS thus enables online convex optimization of this controller, allowing the MPC to shape the disturbance tubes, which in turn yields better optimality, performance, and feasibility. This framework has also been extended in [17] to consider parametric uncertainty in the model, albeit with some conservativeness to preserve convexity. It is further extended to nonlinear systems in [18] by conservatively modelling linearisation errors as parametric uncertainty and employing the method of [17]. Reference [19] employs SLS in a Stochastic MPC framework, as opposed to considering bounded polyhedral disturbances.

The greatest downside in the use of SLS within MPC is its much increased computational complexity, on top of the already significant computational complexity of standard MPC with respect to most other control methods. To tackle this issue, [20] proposes an optimization algorithm specific to a class of SLS-MPC problems and numerically demonstrates its significantly better computational performance with respect to general-purpose solvers. Although structurally different, basic SLS-MPC is equivalent to the affine disturbance feedback method [6, 21], for which a structure-exploiting interior-point optimization algorithm has been proposed [22]. Despite these contributions, the direct deployment of a SLS-MPC to an onboard G&C system could still prove to be challenging due to the limited computational power available for a typical OBC, unless the controller is carefully designed and deployed.

Indeed, we can exploit the unique characteristics of a typical orbital rendezvous mission to design an SLS-MPC formulation and deployment strategy that can, at the least, improve upon the performance of other MPC solutions and, at best, minimize the computational shortcomings of MPC, despite its greater computational complexity. Indeed, we propose *One-Shot* SLS-MPC, which relies on a *single* initial optimization of a nominal trajectory and correction policy to execute a full robust manoeuvre between

two hold points in the rendezvous approach with limited conservativeness and good fuel performance, thus reducing the MPC reliance on *real-time* and *recursive* numerical optimization. Furthermore, this sole optimization can be performed prior to the start of the manoeuvre while maintaining the hold point, which is designed to be safe and potentially time-flexible, such that real-time computation requirements are further softened. To ensure finite-time completion of the manoeuvre, which is important for rendezvous missions which have a pre-determined timeline, we employ the *shrinking-horizon* strategy [2, 8, 23, 24], as opposed to the *receding-horizon* strategy standard in MPC [1].

We consider the far-range rendezvous phase, which typically starts at a relative distance of tens of kilometres and ends at a few hundred meters, and is often characterized by its long duration (up to days) with sparse and relatively short chemical thruster firings, to exploit the natural relative motion to minimize fuel consumption and to ensure a safe relative velocity. Therefore, the MPC prediction model considers a representation of the relative state between the two satellites in terms of relative orbital elements (ROE), namely the formulation proposed by D'Amico [25]. This state representation provides three key advantages, which are particularly useful for the rendezvous phase addressed, with respect to the typical Cartesian models used, e.g., Clohessy-Wiltshire [26] or Yamanaka-Ankersen [27]: 1) more accurate linearisation of the relative dynamics; 2) ease of dynamic modelling of the most relevant perturbations, namely J_2 and atmospheric drag [28]; 3) a simple passive safety concept based on a geometric relation between the ROE state and the shape of the trajectory in Cartesian coordinates [25, 29]. These advantages can be fully exploited by the MPC framework. In particular, the latter is leveraged to formulate a — to the best of our knowledge — novel and simple convex passive safety constraint with limited conservatism. Furthermore, we have derived a novel linearised ROE dynamic model with J_2 and drag perturbations that provides a slight accuracy improvement with respect to the current state-of-the-art linear model of [28]. Overall, the SLS-MPC optimization problem becomes a linear program (LP).

To the best of our knowledge, the main novel contributions of this work are:

- First application of SLS-MPC to rendezvous G&C, including a novel convex robust fuel-optimality metric, highlighting its advantages with respect to practical Robust Tube-Based MPC solutions in terms of optimality, performance, and feasibility.
- Proposal of alternative SLS-MPC deployment strategies, namely One-Shot SLS-MPC, that leverage unique features of rendezvous operations to reduce the dependency of MPC on real-time and recursive numerical optimization.
- Exploitation of an ROE state representation, namely to formulate a novel simple and convex passive safety constraint and a novel J_2- and drag-perturbed linear dynamic model that is a slightly more accurate than the current state of the art.

Section 2 covers the ROE state representation considered by the MPC, including the dynamic model with J_2 and drag perturbations, and the derivation of the proposed passive safety constraint. Section 3 introduces the basic concepts of Robust MPC, and re-iterates a common practical implementation, namely Tube-Based and Linear MPC, as a means for theoretical and numerical comparison with SLS-MPC. Section 4 derives the proposed SLS-MPC formulation and how it can be expressed as an LP-representable optimization problem, and covers the One-Shot SLS-MPC strategy and how it is particularly suitable for the rendezvous problem. Section 5 presents simulation results to demonstrate SLS-MPC and OS-SLS-MPC in a rendezvous scenario and compare them with Linear Tube-Based MPC. Finally, Section 6 concludes the work and presents future research directions.

1.1 Notation

Operators $|\cdot|$ and $\leq$ are interpreted element-wise when applied to vectors. $(*,\ldots,*)$ standalone denotes the vertical concatenation of scalars, vectors, or conformable matrices. e_i is the i-th standard basis vector of conformable dimensions. Depending on the context, vectors and matrices are sometimes, but not always, boldface. $\mathbf{I}_n$ denotes an n-dimensional identity matrix. $\mathbf{1}_n$ is an n-dimensional vector

filled with 1's. $\mathbf{0}_{n\times m}$ is a $n \times m$ matrix filled with 0's. $\mathbb{N}_{[a,b]}$ with $a, b \in \mathbb{N}$ and $b > a \geq 0$ denotes the set $\{a, \ldots, b\}$. $\mathcal{B}_\infty^n$ denotes the n-dimensional infinity-norm ball $\{\xi \in \mathbb{R}^n : \|\xi\|_\infty \leq 1\}$. $\|A\|_{1,1}$ denotes the entry-wise matrix ℓ_1-norm $\sum_{i,j} |A_{ij}|$ of matrix A. $\otimes$ denotes the Kronecker product.

2 Relative Orbital Elements

2.1 Definition

Relative orbital elements (ROE) represent the relative state of two satellites as an algebraic combination of the Keplerian orbital elements of the target satellite $\boldsymbol{\alpha} \coloneqq (a, e, i, \Omega, \omega, M)$ and of the chaser satellite $\boldsymbol{\alpha}_\mathrm{c} \coloneqq (a_\mathrm{c}, e_\mathrm{c}, i_\mathrm{c}, \Omega_\mathrm{c}, \omega_\mathrm{c}, M_\mathrm{c})$. We consider the ROE defined by D'Amico [25]

$$\delta\boldsymbol{\alpha} = \begin{bmatrix} \delta a \\ \delta\lambda \\ \delta e_\mathrm{x} \\ \delta e_\mathrm{y} \\ \delta i_\mathrm{x} \\ \delta i_\mathrm{y} \end{bmatrix} \coloneqq \begin{bmatrix} (a_\mathrm{c} - a)/a \\ u_\mathrm{c} - u + (\Omega_\mathrm{c} - \Omega)\cos(i) \\ e_\mathrm{c}\cos(\omega_\mathrm{c}) - e\cos(\omega) \\ e_\mathrm{c}\sin(\omega_\mathrm{c}) - e\sin(\omega) \\ i_\mathrm{c} - i \\ (\Omega_\mathrm{c} - \Omega)\sin(i) \end{bmatrix}, \tag{1}$$

where $u \coloneqq M + \omega$ is the mean argument of latitude. This formulation is often known as the *quasi-nonsingular* ROE, since it is non-singular for circular orbits but still not uniquely defined for equatorial orbits. A fully nonsingular formulation exists [28], but (1) is simpler and applicable to most scenarios, and is therefore the one adopted here.

This relative state representation provides several advantages with respect to the most common alternatives such as the Clohessy-Wiltshire [26] and Yamanaka-Ankersen [27, 30] models, based on Cartesian coordinates in the *local-vertical/local-horizontal* (LVLH) frame. We highlight three such advantages that are particularly useful for the present application and which can be fully exploited by the MPC framework: 1) more accurate and simpler linearised dynamics; 2) ease of dynamic modelling of the most relevant perturbations, namely first-order J_2 and atmospheric drag [28]; 3) simple passive safety concept based on the geometric relation between the ROE state and the shape of the trajectory in Cartesian coordinates, namely the separation of the relative eccentricity and inclination (E/I) vectors [25, 29]. In particular, the latter is leveraged in Section 2.4 to formulate a simple convex passive safety constraint with limited conservatism. Furthermore, we derive in Section 2.2 a novel linearised ROE dynamic model with J_2 and drag perturbations that provides a slight accuracy improvement with respect to the current state-of-the-art linear model of [28].

Remark 1. In the following sections, the absolute orbital elements $\boldsymbol{\alpha}$ and $\boldsymbol{\alpha}_c$ and the relative orbital elements $\delta\boldsymbol{\alpha}$ always denote J_2-*mean* orbital elements, i.e., which disregard the periodic effects of first-order J_2 perturbations, as opposed to *osculating* elements. A method for converting from mean to osculating elements can be found in [31, §9.9.1]. The converse transformation requires numerical algorithms, of which a good example is found in [32].

2.2 Dynamic Model

We next present a discrete-time linear dynamic model for the ROE formulation (1) that includes: control ΔVs, target orbit eccentricity, and J_2 and drag perturbations. The model is based on a modification of the density-model-free state transition matrix (STM) for arbitrary eccentricity in [28, §VIII], which augments the state vector with the derivatives of the relative semi-major axis and relative eccentricity due to drag, denoted $(\delta\dot{a}_\mathrm{drag}, \delta\dot{e}_\mathrm{x,drag}, \delta\dot{e}_\mathrm{y,drag})$.

2.2.1 Free Regime with J_2 and Drag Perturbations

We consider a different modified ROE linear transformation — that is used to enable a simpler solution method for the differential equations for the linearised dynamics — with respect to that considered in [28, §VIII] that accounts for the modified ROEs in the augmented state vector, yielding

$$\bar{\mathbf{J}}(\boldsymbol{\alpha}) \coloneqq \left[\begin{array}{cccccc|ccc} & & & \mathbf{J}(\boldsymbol{\alpha}) & & & & \mathbf{0}_{6\times3} & \\ \hline 0 & 0 & 0 & 0 & 0 & 0 & 1 & 0 & 0 \\ 0 & 0 & -\dot{\omega}\sin\omega & \dot{\omega}\cos\omega & 0 & 0 & 0 & \cos\omega & \sin\omega \\ 0 & 0 & -\dot{\omega}\cos\omega & -\dot{\omega}\sin\omega & 0 & 0 & 0 & -\sin\omega & \cos\omega \end{array}\right], \tag{2}$$

where $\mathbf{J}(\boldsymbol{\alpha})$ is the same as in [28, eq. (20)]. Therefore, this yields the following STM for the state at time t to that at time $t + \Delta t$ as a function of the initial target orbital elements $\boldsymbol{\alpha}(t)$

$$\boldsymbol{\Phi}_{\mathrm{J}_2+\mathrm{drag}}(\boldsymbol{\alpha}(t)) = \begin{bmatrix} \boldsymbol{\Phi}_{\mathrm{J}_2}(\boldsymbol{\alpha}(t)) & \bar{\boldsymbol{\Phi}}_{\mathrm{J}_2+\mathrm{drag}}(\boldsymbol{\alpha}(t)) \\ \mathbf{0}_{3\times6} & \mathbf{I}_3 \end{bmatrix}, \tag{3}$$

where $\boldsymbol{\Phi}_{\mathrm{J}_2}(\boldsymbol{\alpha}(t))$ is the same as [28, eq. (A6)], repeated next for completion

$$\boldsymbol{\Phi}_{\mathrm{J}_2}(\boldsymbol{\alpha}(t)) \coloneqq \begin{bmatrix} 1 & 0 & 0 & 0 & 0 & 0 \\ -(\frac{3}{2}n + \frac{7}{2}\kappa EP)\Delta t & 1 & \kappa e_{\mathrm{x}} FGP\Delta t & \kappa e_{\mathrm{y}} FGP\Delta t & -\kappa FS\Delta t & 0 \\ \frac{7}{2}\kappa e_{\mathrm{y,f}} Q\Delta t & 0 & \cos(\dot{\omega}\Delta t) - 4\kappa e_{\mathrm{x}} e_{\mathrm{y,f}} GQ\Delta t & -\sin(\dot{\omega}\Delta t) - 4\kappa e_{\mathrm{y}} e_{\mathrm{y,f}} GQ\Delta t & 5\kappa e_{\mathrm{y,f}} S\Delta t & 0 \\ -\frac{7}{2}\kappa e_{\mathrm{x,f}} Q\Delta t & 0 & \sin(\dot{\omega}\Delta t) + 4\kappa e_{\mathrm{x}} e_{\mathrm{x,f}} GQ\Delta t & \cos(\dot{\omega}\Delta t) + 4\kappa e_{\mathrm{y}} e_{\mathrm{x,f}} GQ\Delta t & -5\kappa e_{\mathrm{x,f}} S\Delta t & 0 \\ 0 & 0 & 0 & 0 & 1 & 0 \\ \frac{7}{2}\kappa S\Delta t & 0 & -4\kappa e_{\mathrm{x}} GS\Delta t & -4\kappa e_{\mathrm{y}} GS\Delta t & 2\kappa T\Delta t & 1 \end{bmatrix}, \tag{4}$$

with

$$\begin{gathered} n \coloneqq \sqrt{\frac{\mu}{a^3}}, \quad e_{\mathrm{x}} \coloneqq e\cos\omega, \quad e_{\mathrm{y}} \coloneqq e\sin\omega, \quad e_{\mathrm{x,f}} \coloneqq e\cos\omega_{\mathrm{f}}, \quad e_{\mathrm{y,f}} \coloneqq e\sin\omega_{\mathrm{f}}, \\ \dot{\omega} \coloneqq \kappa Q, \quad \omega_{\mathrm{f}} \coloneqq \omega + \dot{\omega}\Delta t, \quad \eta \coloneqq \sqrt{1-e^2}, \quad \kappa \coloneqq \frac{3}{4}\frac{J_2 R_E^2 \sqrt{\mu}}{a^{7/2}\eta^4}, \quad E \coloneqq 1+\eta, \quad F \coloneqq 4+3\eta, \\ G \coloneqq \frac{1}{\eta^2}, \quad P \coloneqq 3\cos^2 i - 1, \quad Q \coloneqq 5\cos^2 i - 1, \quad S \coloneqq \sin(2i), \quad T \coloneqq \sin^2 i, \end{gathered} \tag{5}$$

where (a, e, i, ω) pertain to the initial target elements $\boldsymbol{\alpha}(t)$, and where

$$\bar{\boldsymbol{\Phi}}_{\mathrm{J}_2+\mathrm{drag}}(\boldsymbol{\alpha}(t)) \coloneqq \begin{bmatrix} \Delta t & 0 & 0 \\ -(\frac{3}{4}n + \frac{7}{4}\kappa EP)\Delta t^2 & \frac{1}{2}\kappa e_{\mathrm{x}} FGP\Delta t^2 & \frac{1}{2}\kappa e_{\mathrm{y}} FGP\Delta t^2 \\ \frac{7}{4}\kappa e_{\mathrm{y,f}} Q\Delta t^2 & \cos(\dot{\omega}\Delta t)\Delta t - 2\kappa e_{\mathrm{x}} e_{\mathrm{y,f}} GQ\Delta t^2 & -\sin(\dot{\omega}\Delta t)\Delta t - 2\kappa e_{\mathrm{y}} e_{\mathrm{y,f}} GQ\Delta t^2 \\ -\frac{7}{4}\kappa e_{\mathrm{x}} Q\Delta t^2 & \sin(\dot{\omega}\Delta t)\Delta t + 2\kappa e_{\mathrm{x}} e_{\mathrm{x,f}} GQ\Delta t^2 & \cos(\dot{\omega}\Delta t)\Delta t + 2\kappa e_{\mathrm{y}} e_{\mathrm{x,f}} GQ\Delta t^2 \\ 0 & 0 & 0 \\ \frac{7}{4}\kappa S\Delta t^2 & -2\kappa e_{\mathrm{x}} GS\Delta t^2 & -2\kappa GSe_{\mathrm{y}}\Delta t^2 \end{bmatrix}. \tag{6}$$

Remark 2. When J_2 is set to zero then (6) recovers the drag STM without J_2 in [28, eq. (77)], which does not occur for the STM [28, eq. (D2)]. This is due to the modified ROE transformation (2) accounting in $(\delta\dot{e}_{\mathrm{x,drag}}, \delta\dot{e}_{\mathrm{y,drag}})$ for the effect of the the transformation of $(\delta e_{\mathrm{x}}, \delta e_{\mathrm{y}})$ due to $\mathbf{J}(\cdot)$, which is not the case in the latter. Consequently, (6) is also slightly more accurate than [28, eq. (D2)].

Given that the augmented state variables $(\delta\dot{a}_{\mathrm{drag}}, \delta\dot{e}_{\mathrm{x,drag}}, \delta\dot{e}_{\mathrm{y,drag}})$ are assumed independent of $\delta\boldsymbol{\alpha}(t)$ in (3), as is in [28], these parameters may be handled as an additive term in the dynamic equations rather than true state variables, which reduces the dimensions of the MPC problems in Sections 3 and 4. Furthermore, we derive explicit approximate expressions for these parameters via the Gauss Variational Equations [31, §9.3.2], considering the approximate relative drag acceleration

$$\delta\boldsymbol{\gamma}_{\mathrm{drag}}(\boldsymbol{\alpha}) \coloneqq \frac{1}{2}\rho(\boldsymbol{\alpha})\delta B\|\mathbf{v}_{\mathrm{rel}}(\boldsymbol{\alpha})\|_2\mathbf{R}_{\mathrm{ECI}}^{\mathrm{LVLH}}(\boldsymbol{\alpha})\mathbf{v}_{\mathrm{rel}}(\boldsymbol{\alpha}), \tag{7}$$

where ρ is the atmospheric density at the target satellite position, $\delta B \coloneqq B_{\mathrm{c}} - B$ is the relative inverse ballistic coefficient of the two satellites ($B \coloneqq C_{\mathrm{D}}S/m$), $\mathbf{v}_{\mathrm{rel}}$ is the orbital velocity vector of the target satellite with respect to the atmosphere given by

$$\mathbf{v}_{\mathrm{rel}} = \mathbf{v} - \mathbf{v}_{\mathrm{atm}}, \tag{8}$$

where $\mathbf{v}$ is the target spacecraft inertial velocity vector expressed in the Earth-centred inertial (ECI) frame and $\mathbf{v}_{\mathrm{atm}}$ is the atmosphere velocity vector, and $\mathbf{R}_{\mathrm{ECI}}^{\mathrm{LVLH}}$ is the rotation matrix from the inertial frame to the local orbital frame [10, §3.1.3]. Under the assumption that the atmosphere rotates perfectly with the Earth angular velocity vector and that its rotation axis is exactly aligned with the Z-axis of the ECI frame we have

$$\mathbf{v}_{\mathrm{atm}} = (0, 0, \omega_{\mathrm{Earth}}) \times \mathbf{r}, \tag{9}$$

where ω_{Earth} is the angular velocity of the Earth rotation and $\mathbf{r}$ is the target spacecraft inertial position.

For a zeroth-order Taylor series approximation about the target orbital parameters yields

$$\delta\dot{\boldsymbol{\alpha}}_{\mathrm{drag}}(\boldsymbol{\alpha}) \approx \mathbf{B}_{\mathrm{drag}}(\boldsymbol{\alpha})\delta\boldsymbol{\gamma}_{\mathrm{drag}}(\boldsymbol{\alpha}), \tag{10}$$

where $\delta\dot{\boldsymbol{\alpha}}_{\mathrm{drag}} \coloneqq (\delta\dot{a}_{\mathrm{drag}}, \delta\dot{e}_{\mathrm{x,drag}}, \delta\dot{e}_{\mathrm{y,drag}})$, and

$$\mathbf{B}_{\mathrm{drag}}(\boldsymbol{\alpha}) \coloneqq \frac{1}{an}\begin{bmatrix} \frac{2}{\eta}(1+e\cos\theta) & 0 & -\frac{2}{\eta}e\sin\theta \\ \eta\frac{(2+e\cos\theta)\cos\nu+e_{\mathrm{x}}}{1+e\cos\theta} & -\frac{\eta e_{\mathrm{y}}}{\tan i}\frac{\sin\nu}{1+e\cos\theta} & -\eta\sin\nu \\ \eta\frac{(2+e\cos\theta)\sin\nu+e_{\mathrm{y}}}{1+e\cos\theta} & \frac{\eta e_{\mathrm{x}}}{\tan i}\frac{\sin\nu}{1+e\cos\theta} & \eta\cos\nu \end{bmatrix}, \tag{11}$$

where $\nu \coloneqq \theta + \omega$ is the true argument of latitude.

For the MPC dynamic model used in later sections, a different STM must be computed for each discretization node, which requires propagating the mean target orbital elements. For simplification, we disregard drag in this propagation, and consider only the basic Keplerian motion and the first-order J_2 (secular) effects, for which yield constant drift rates of the mean elements (Ω, ω, M), such that $\boldsymbol{\alpha}(t)$ is

propagated with [28, eq. (13)]

$$\boldsymbol{\alpha}(t+\Delta t) \approx \boldsymbol{\alpha}(t) + \begin{bmatrix} 0 \\ 0 \\ 0 \\ -2\kappa\cos i \\ \kappa(5\cos^2 i - 1) \\ n + \kappa\eta(3\cos^2 i - 1) \end{bmatrix} \Delta t. \tag{12}$$

From the propagated target mean orbital elements, the relative drag acceleration (7) can be computed by converting them to osculating elements [31, §9.9.1], converting to ECI Cartesian coordinates to obtain $(\mathbf{r}, \mathbf{v})$, and computing the rotation matrix $\mathbf{R}_{\text{ECI}}^{\text{LVLH}}$. The atmospheric density ρ can also be computed at each sample with any desired model; in Section 5 we consider the NRLMSISE-00 model, that first requires converting the ECI position to latitude, longitude, altitude (LLA) geodetic coordinates.

2.2.2 Impulsive Forced Regime

The control variable is parametrized as an instant change in velocity, or ΔV, denoted by $\delta\mathbf{v}(t)$, expressed in the LVLH frame. We consider a model similar to that in [33, eq. (13)] but for the ROE formulation (1), rather than the eccentric ROE formulation considered there, to ensure compatibility with the STM derived in Section 2.2.1. Thus yields the control/input matrix

$$\mathbf{B}(\boldsymbol{\alpha}) \coloneqq \frac{1}{an} \begin{bmatrix} \frac{2}{\eta}(1+e\cos\theta) & 0 & -\frac{2}{\eta}e\sin\theta \\ \eta\frac{1-\eta}{e}\left(1+\frac{1}{1+e\cos\theta}\right)\sin\theta & 0 & \eta\left(\frac{2\eta}{1+e\cos\theta}+\frac{1-\eta}{e}\cos\theta\right) \\ \eta\frac{(2+e\cos\theta)\cos\nu+e_{\text{x}}}{1+e\cos\theta} & -\frac{\eta e_{\text{y}}}{\tan i}\frac{\sin\nu}{1+e\cos\theta} & -\eta\sin\nu \\ \eta\frac{(2+e\cos\theta)\sin\nu+e_{\text{y}}}{1+e\cos\theta} & \frac{\eta e_{\text{x}}}{\tan i}\frac{\sin\nu}{1+e\cos\theta} & \eta\cos\nu \\ 0 & -\eta\frac{\cos\nu}{1+e\cos\theta} & 0 \\ 0 & -\eta\frac{\sin\nu}{1+e\cos\theta} & 0 \end{bmatrix}, \tag{13}$$

which we note to have its first, third, and fourth rows in common with $\mathbf{B}_{\text{drag}}$.

Remark 3. The non-zero entries in the second row of $B(\cdot)$ in (13) possess numerical singularities for $e = 0$, which come directly from the Gauss Variational Equations from which it is derived, and which is the reason behind the use of the alternative ROE formulation in [33]. Nonetheless, (13) was found to remain numerically stable even for very small eccentricities of $e > 10^{-6}$.

The full linear time-varying state-space model is thus

$$\delta\boldsymbol{\alpha}(t+\Delta t) = \boldsymbol{\Phi}_{\text{J}_2}(\boldsymbol{\alpha}(t))\left(\delta\boldsymbol{\alpha}(t) + \mathbf{B}(\boldsymbol{\alpha}(t))\delta\mathbf{v}(t)\right) + \bar{\boldsymbol{\Phi}}_{\text{J}_2+\text{drag}}(\boldsymbol{\alpha}(t))\mathbf{B}_{\text{drag}}(\boldsymbol{\alpha}(t))\delta\boldsymbol{\gamma}_{\text{drag}}(\boldsymbol{\alpha}(t)). \tag{14}$$

2.3 Geometric Interpretation

One desirable characteristic of the ROE formulation (1) is its direct geometric relation with the resulting relative trajectory expressed in LVLH, with the assumption of a near-circular target orbit and the absence of perturbations [25]. Indeed, in these conditions, there exists an accurate linearised mapping

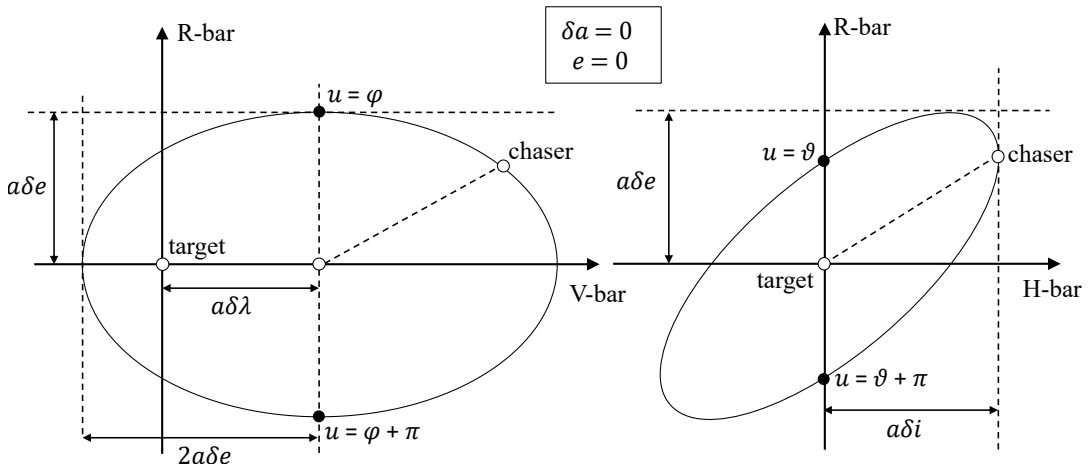

Fig. 1 Geometric relation between the relative orbital elements and the LVLH trajectory for $e = 0$ and $\delta a = 0$. Left: V-bar/R-bar plane. Right: H-bar/R-bar plane.

between the ROE (1) and the LVLH position (x, y, z), given by [25]

$$\begin{bmatrix} x \\ y \\ z \end{bmatrix} \approx \begin{bmatrix} 0 & 1 & 2\sin u & -2\cos u & 0 & 0 \\ 0 & 0 & 0 & 0 & -\sin u & \cos u \\ -1 & 0 & \cos u & \sin u & 0 & 0 \end{bmatrix} a\delta\boldsymbol{\alpha}. \tag{15}$$

Furthermore, in the unperturbed case ($J_2 = \delta B = 0$), the STM (4) becomes

$$\boldsymbol{\Phi}(\Delta t) = \begin{bmatrix} 1 & 0 & 0 & 0 & 0 & 0 \\ -\frac{3}{2}n\Delta t & 1 & 0 & 0 & 0 & 0 \\ 0 & 0 & 1 & 0 & 0 & 0 \\ 0 & 0 & 0 & 1 & 0 & 0 \\ 0 & 0 & 0 & 0 & 1 & 0 \\ 0 & 0 & 0 & 0 & 0 & 1 \end{bmatrix}, \tag{16}$$

and we also have $\delta\dot{\boldsymbol{\alpha}}_{\text{drag}} = 0$, $(\dot{a}, \dot{e}, \dot{i}, \dot{\Omega}, \dot{\omega}) = 0$, and $\dot{M} = n$ constant, meaning that all ROE states save for $\delta\lambda$ remain constant with time. Thus, together with the fact that $(\delta e_{\text{x}}, \delta e_{\text{y}}, \delta i_{\text{x}}, \delta i_{\text{y}})$ multiply time-dependent cosine/sine terms in (15), it is readily apparent that the LVLH trajectory has an elliptical motion parametrized by the ROE state. This is illustrated in Figure 1 for $\delta a = 0$, in which case the trajectory is a closed/static ellipse that is centred on the V-bar axis with an offset of $a\delta\lambda$ along it. To better understand this parametrization, it is convenient to express the relative eccentricity and inclination (E/I) vectors in polar coordinates

$$\delta\mathbf{e} := \begin{bmatrix} \delta e_x \\ \delta e_y \end{bmatrix} = \delta e \begin{bmatrix} \cos(\varphi) \\ \sin(\varphi) \end{bmatrix}, \qquad \delta\mathbf{i} := \begin{bmatrix} \delta i_x \\ \delta i_y \end{bmatrix} = \delta i \begin{bmatrix} \cos(\vartheta) \\ \sin(\vartheta) \end{bmatrix}. \tag{17}$$

Figure 1 thus shows that the dimensions of the ellipse depend on the magnitudes $(\delta e, \delta i)$ of these vectors, and that its orientation in space depends on their angles (φ, ϑ).

For $\delta a \neq 0$, two effects occur: the centre of the ellipse is offset along R-bar by a distance of $-a\delta a$, and the ellipse drifts along V-bar with time, given that $a\delta a$ induces a drift of $\delta\lambda$ in (16). This motion is known as the "travelling/walking ellipse" [10, §A.1.5], and is illustrated in Figure 2. Whether or not the ellipse is indeed travelling, its projection to the H-bar/R-bar plane is still a closed ellipse, a fact that is exploited for verifying and ensuring passive safety in Section 2.4.

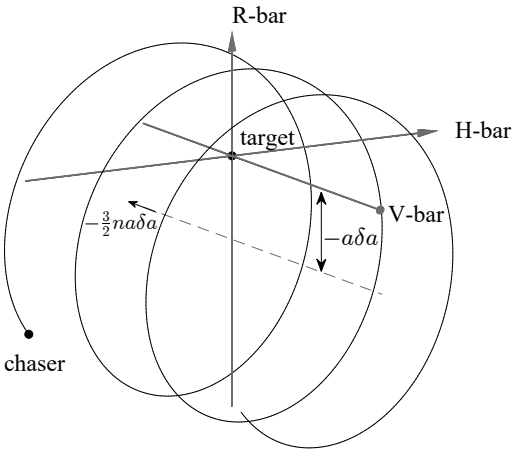

Fig. 2 Geometric relation between the relative orbital elements and the LVLH trajectory for $e = 0$ and $\delta a > 0$.

2.4 Passive Safety Concept

2.4.1 Definition

Rendezvous trajectories must typically be designed to be *passively safe*, whereby the free-drift trajectory resulting from any point in the nominal trajectory — e.g., due to loss of actuators or OBC — does not lead, within a specified time-horizon, to a collision with the target S/C or, more conservatively, to a violation of a keep-out-zone [10]. Formulating passive safety constraints in terms of Cartesian coordinates is challenging for two main reasons:

1) Even for the nominal trajectory, a collision avoidance constraint is non-convex, which can be handled by mixed-integer programming [34], or via convex relaxations that may lead to significant conservatism, e.g., a half-space relaxation [35], or which are applicable only in specific proximity scenarios, e.g., a time-variant half-space relaxation that follows the docking port of a rotating target S/C [36, 37]
2) Extending these constraints to passive safety has been achieved by:
    - Sampling each point of the nominal trajectory and constraining their respective propagated free-drift/failure trajectories for the required time-horizon and discretization granularity [8, 35], which scales poorly with the prediction horizon and the passive safety horizon;
    - Forcing orbit-invariant failure trajectories to ensure an indefinite safety horizon at the cost of significant conservatism [35];
    - Via semi-definite programming (SDP) to avoid discretizing the failure trajectories [38], which may also become computationally expensive for onboard deployment.

A simple passive safety concept arises by leveraging a rendezvous approach with travelling-ellipse type trajectories, and the fact that, for the assumptions in Section 2.3, such trajectories are parametrized by a single ROE state. Therefore, the ROE state readily parametrizes a relative *trajectory* rather than an instantaneous relative position, which can be exploited to formulate a passive safety constraint without sampling the failure trajectories. Namely, since the free-drift ellipse is invariant in H-bar/R-bar and only drifts along V-bar as illustrated in Figure 2, passive safety is ensured as long as the ellipse clears the V-bar axis with sufficient distance. This depends on two factors: the magnitude $(\delta e, \delta i)$ of the relative E/I vectors, and on the phase $\varphi - \vartheta$ between them. As illustrated in Figure 3, the clearance of the ellipse to the V-bar axis is maximized for parallel relative E/I vectors. Furthermore, for $\delta a \neq 0$ the ellipse is offset along R-bar by $-a\delta a$ as illustrated in Figure 2, which thus also affects the clearance from V-bar.

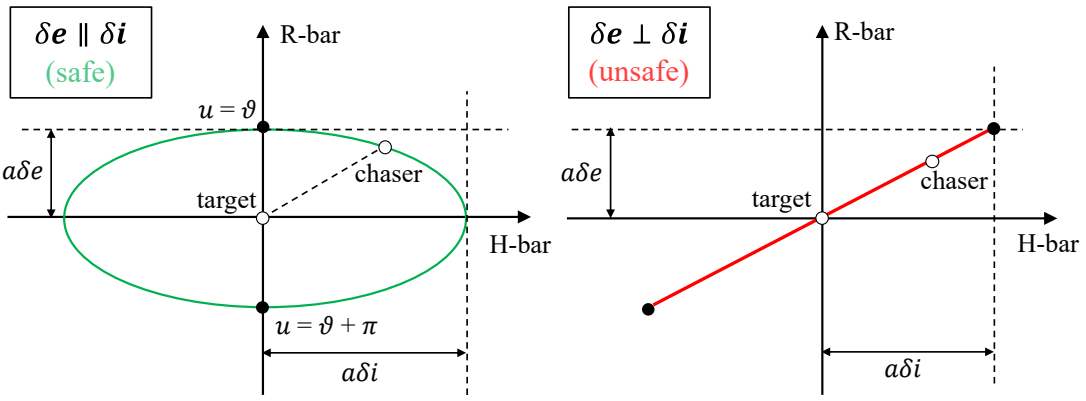

Fig. 3 Orientation of the ellipse in the H-bar/R-bar plane depending on the phase of the relative eccentricity and inclination vectors, for $e = \delta a = 0$.

For a given ROE state, the relative distance from the V-bar axis along H-bar and R-bar can be approximately computed using the linear mapping (15) assuming an unperturbed and circular target orbit, yielding (cf. [25, eq. (2.21)])

$$d_{\mathrm{HR}}(u, \delta\boldsymbol{\alpha}) \coloneqq a\sqrt{(\delta e_{\mathrm{x}} \cos(u) + \delta e_{\mathrm{y}} \sin(u) - \delta a)^2 + (\delta i_{\mathrm{y}} \cos(u) - \delta i_{\mathrm{x}} \sin(u))^2}. \tag{18}$$

In the absence of perturbations, the ROEs $(\delta a, \delta\mathbf{e}, \delta\mathbf{i})$ are constant in time (cf. (16)), and therefore the minimum possible HR distance along time is given by

$$d_{\mathrm{HR}}^{\min}(\delta\boldsymbol{\alpha}) \coloneqq \min_{u\in[0,2\pi]} d_{\mathrm{HR}}(u, \delta\boldsymbol{\alpha}). \tag{19}$$

Therefore, passive safety can be ensured by enforcing the constraint

$$d_{\mathrm{HR}}^{\min}(\delta\boldsymbol{\alpha}) \geq d_{\mathrm{safe}} \tag{20}$$

on all relative states $\delta\boldsymbol{\alpha}$ along a trajectory, and for a sufficiently great safety distance $d_{\mathrm{safe}} \in \mathbb{R}_{++}$. The distance d_{safe} is a design parameter that is assumed here to include appropriate margins that account for eccentricity in the target orbit, which deforms the walking ellipse, and environmental perturbations, which challenge the assumption that the ROEs in (18) remain constant with time.

For $\delta a = 0$, the minimization (19) has a simple optimal value given by (cf. [25, eq. (2.22)])

$$\bar{d}_{\mathrm{HR}}^{\min}(\delta\boldsymbol{\alpha}) \coloneqq \min_{u\in[0,2\pi]} \bar{d}_{\mathrm{HR}}(u, \delta\boldsymbol{\alpha}) = \frac{1}{2} a \left| \|\delta\mathbf{e} + \delta\mathbf{i}\|_2 - \|\delta\mathbf{e} - \delta\mathbf{i}\|_2 \right|, \tag{21}$$

where $\bar{d}_{\mathrm{HR}}(u, \delta\boldsymbol{\alpha}) \coloneqq d_{\mathrm{HR}}(u, \delta\boldsymbol{\alpha})\big|_{\delta a=0}$. In the general case, however, the minimum value (19) instead requires computing the roots of a fourth-order polynomial [29], which is not favourable for formulating the optimization constraint based on (20). We thus seek a closed-form approximation instead, which must be conservative, given the importance of this constraint for the safety of the spacecraft.

2.4.2 Closed-Form Approximation

The following result provides a conservative approximation to the passive safety constraint (20) that can be formulated in closed-form.

Proposition 1. *Let $\bar{d}^{\min}_{\mathrm{HR}}(\delta\boldsymbol{\alpha})$ and $\bar{d}^{\max}_{\mathrm{HR}}(\delta\boldsymbol{\alpha})$ denote the min/max values of $\bar{d}_{\mathrm{HR}}(u, \delta\boldsymbol{\alpha})$ when $\delta a = 0$, with the former given in* (21) *and the latter given by*

$$\bar{d}^{\max}_{\mathrm{HR}}(\delta\boldsymbol{\alpha}) = \frac{1}{2}a\left|\|\delta\mathbf{e} + \delta\mathbf{i}\|_2 + \|\delta\mathbf{e} - \delta\mathbf{i}\|_2\right|. \tag{22}$$

A conservative lower-bound for the minimum $d^{\min}_{\mathrm{HR}}(\delta\boldsymbol{\alpha})$ is

$$\hat{d}^{\min}_{\mathrm{HR}}(\delta\boldsymbol{\alpha}) \coloneqq \begin{cases} 0, & a|\delta a| \in [\bar{d}^{\min}_{\mathrm{HR}}(\delta\boldsymbol{\alpha}), \bar{d}^{\max}_{\mathrm{HR}}(\delta\boldsymbol{\alpha})] \\ \bar{d}^{\min}_{\mathrm{HR}}(\delta\boldsymbol{\alpha}) - a|\delta a|, & a|\delta a| < \bar{d}^{\min}_{\mathrm{HR}}(\delta\boldsymbol{\alpha}) \\ a|\delta a| - \bar{d}^{\max}_{\mathrm{HR}}(\delta\boldsymbol{\alpha}), & a|\delta a| > \bar{d}^{\max}_{\mathrm{HR}}(\delta\boldsymbol{\alpha}) \end{cases} \tag{23}$$

such that enforcing

$$\hat{d}^{\min}_{\mathrm{HR}}(\delta\boldsymbol{\alpha}) \geq d_{\mathrm{safe}} \tag{24}$$

implies (20)*.*

Proof. Apply the reverse triangle inequality to $d_{\mathrm{HR}}(\cdot)$, which yields the lower-bound

$$d_{\mathrm{HR}}(u, \delta\boldsymbol{\alpha}) \geq \left|\bar{d}_{\mathrm{HR}}(u, \delta\boldsymbol{\alpha}) - a|\delta a|\right|, \tag{25}$$

that we wish to minimize over $u \in [0, 2\pi]$ as in (19). Notice that $\bar{d}_{\mathrm{HR}}(u, \delta\boldsymbol{\alpha}) \in [\bar{d}^{\min}_{\mathrm{HR}}(\delta\boldsymbol{\alpha}), \bar{d}^{\max}_{\mathrm{HR}}(\delta\boldsymbol{\alpha})]$, with $\bar{d}^{\min}_{\mathrm{HR}}(\delta\boldsymbol{\alpha})$ and $\bar{d}^{\max}_{\mathrm{HR}}(\delta\boldsymbol{\alpha})$ previously defined in (21) and (22). The minimum of the lower-bound (25) can thus be determined by evaluating the three different cases in (23), which are individually trivial to solve. □

2.4.3 Convex Approximation

Despite $\hat{d}^{\min}_{\mathrm{HR}}(\delta\boldsymbol{\alpha})$ being a closed-form lower-bound for $d^{\min}_{\mathrm{HR}}(\delta\boldsymbol{\alpha})$, it is still a non-convex function of $\delta\boldsymbol{\alpha}$. Thus, further simplification is desirable for embedding efficiently as an optimization constraint.

Proposition 2. *Let $\delta\mathbf{w} \in \mathbb{R}^2$ be a unit vector. If $\tilde{d}^{\min}_{\mathrm{HR}}(\delta\boldsymbol{\alpha}) \geq d_{\mathrm{safe}}$ with*

$$\tilde{d}^{\min}_{\mathrm{HR}}(\delta\boldsymbol{\alpha}) \coloneqq \frac{1}{2}a\delta\mathbf{w}^{\mathrm{T}}(\delta\mathbf{e} + \delta\mathbf{i}) - a\left(|\delta a| + \frac{1}{2}\|\delta\mathbf{e} - \delta\mathbf{i}\|_2\right), \tag{26}$$

then (20) *holds, as well as $a|\delta a| < \bar{d}^{\min}_{\mathrm{HR}}(\delta\boldsymbol{\alpha})$ and $|\varphi - \vartheta| \leq \pi/2$.*

Proof. Limiting $\delta\boldsymbol{\alpha}$ to the first case $a|\delta a| < \bar{d}^{\min}_{\mathrm{HR}}(\delta\boldsymbol{\alpha})$ in (23), then the passive safety constraint becomes

$$\bar{d}^{\min}_{\mathrm{HR}}(\delta\boldsymbol{\alpha}) = \frac{1}{2}a\left|\|\delta\mathbf{e} + \delta\mathbf{i}\|_2 - \|\delta\mathbf{e} - \delta\mathbf{i}\|_2\right| \geq d_{\mathrm{safe}} + a|\delta a|, \tag{27}$$

which implies $a|\delta a| < \bar{d}^{\min}_{\mathrm{HR}}(\delta\boldsymbol{\alpha})$ and thus (24), and is still non-convex in $\delta\boldsymbol{\alpha}$. Further restricting the relative trajectory to the case $\|\delta\mathbf{e} + \delta\mathbf{i}\|_2 \geq \|\delta\mathbf{e} - \delta\mathbf{i}\|_2$, or equivalently $|\varphi - \vartheta| \leq \pi/2$ eliminates the absolute value in the LHS of (27), yielding

$$\frac{1}{2}a\|\delta\mathbf{e} + \delta\mathbf{i}\|_2 \geq d_{\mathrm{safe}} + a\left(|\delta a| + \frac{1}{2}\|\delta\mathbf{e} - \delta\mathbf{i}\|_2\right), \tag{28}$$

which implies $\|\delta\mathbf{e} + \delta\mathbf{i}\|_2 \geq \|\delta\mathbf{e} - \delta\mathbf{i}\|_2$ and thus (27), and which is still non-convex due to the norm on the LHS. Linearising this norm about a unit vector $\delta\mathbf{w} \in \mathbb{R}^2$ yields $\|\delta\mathbf{e} + \delta\mathbf{i}\|_2 \approx \delta\mathbf{w}^{\mathrm{T}}(\delta\mathbf{e} + \delta\mathbf{i})$. Since

any norm is a convex function, its linearisation is a guaranteed lower-bound, and thus (26) implies (24), which by Proposition 1 implies (20). □

Remark 4. Notice that the three cases in (23) correspond to, in their respective order: 1) the walking ellipse potentially colliding with the V-bar axis, although not necessarily so given the prior approximation; 2) the walking ellipse strictly circling the V-bar axis; 3) the walking ellipse being strictly above or below (along R-bar) the V-bar axis. Therefore, the conservativeness of restricting the relative trajectory to the second case, as done in Proposition 2, may be limited if the initial and desired ROEs are designed likewise. Similarly, the conservativeness of restricting the state to $|\varphi - \vartheta| \leq \pi/2$ and of the norm linearisation may be minimized by designing both the initial relative E/I vectors to be parallel to each other ($\varphi = \vartheta$), as well as parallel to the desired E/I vector and the linearisation unit vector $\delta\mathbf{w}$.

The conservative passive constraint set (26) is now convex in $\delta\boldsymbol{\alpha}$, and, in particular, representable in $(|\delta a|, \delta\mathbf{e}, \delta\mathbf{i})$ as a second-order cone [39, §2.2.3]. Nonetheless, the constraint tightening approaches performed for MPC later in Sections 3 and 4 are more amenable to linear constraints; thus constraint (26) is next approximated one last time.

Lemma 3. *Let $\delta\mathbf{w} \in \mathbb{R}^2$ be a unit vector. If $\tilde{d}_{\mathrm{HR}}^{\min,\infty}(\delta\boldsymbol{\alpha}) \geq d_{\mathrm{safe}}$*

$$\tilde{d}_{\mathrm{HR}}^{\min,\infty}(\delta\boldsymbol{\alpha}) \coloneqq \frac{1}{2}a\delta\mathbf{w}^{\mathrm{T}}(\delta\mathbf{e} + \delta\mathbf{i}) - a\left(|\delta a| + \frac{\sqrt{2}}{2}\|\delta\mathbf{e} - \delta\mathbf{i}\|_\infty\right), \tag{29}$$

then (20) *holds.*

Proof. Apply Hölder's inequality $\sqrt{2}\|\mathbf{v}\|_\infty \geq \|\mathbf{v}\|_2$ to the norm in the RHS of (26) and use Propositions 2 and 1. □

Thus, the inequality (29) conservatively models a convex and polyhedral passive safety constraint. One way to reformulate (29) explicitly as a linear inequality is

$$C_{\mathrm{safe}}\delta\boldsymbol{\alpha} \leq b_{\mathrm{safe}}, \tag{30}$$

where $b_{\mathrm{safe}} = -d_{\mathrm{safe}}\mathbf{1}_8$ and

$$C_{\mathrm{safe}} = a\begin{bmatrix} \mathbf{1}_4 & \mathbf{0}_{4\times1} & \bar{C}_{\mathrm{safe}} \\ -\mathbf{1}_4 & \mathbf{0}_{4\times1} & \bar{C}_{\mathrm{safe}} \end{bmatrix} \tag{31}$$

with $\bar{C}_{\mathrm{safe}} = \frac{1}{2}\left(\mathbf{1}_{4\times2} \otimes \delta\mathbf{w}^{\mathrm{T}} + \sqrt{2}\,[\mathbf{I}_2 \;\; -\mathbf{I}_2] \otimes \left[\begin{smallmatrix}1\\-1\end{smallmatrix}\right]\right)$.

Figure 4 illustrates the resulting passive safety constraint sets for the original minimum HR distance metric $d_{\mathrm{HR}}^{\min}$, the simplified closed-form metric $\hat{d}_{\mathrm{HR}}^{\min}$, and the convexified metric $\tilde{d}_{\mathrm{HR}}^{\min,\infty}$, from which it can be observed that each one is subset of the previous and thus conservative approximations. It is also remarked that, although the first two sets appear convex in the left plot in terms of the relative E/I vectors' magnitude and phase for a small fixed δa, it is actually not so with respect to the Cartesian components of these vectors. The left plot also highlights how the approximate sets conservatively assume that $\delta\mathbf{i}$ is constrained by $\delta a \neq 0$ similarly to $\delta\mathbf{e}$, which is due to the simplification in (24). The right plot shows two disconnected regions of the set, where the leftmost region corresponds to the case where the ellipse lies above or below the V-bar axis along R-bar, and the rightmost region corresponds to the case where the ellipse orbits the V-bar axis, which is the one selected for the convexified set. Finally, it is observed that the approximate sets are the least conservative when the E/I vectors' phase is 0 and their magnitudes are the same.

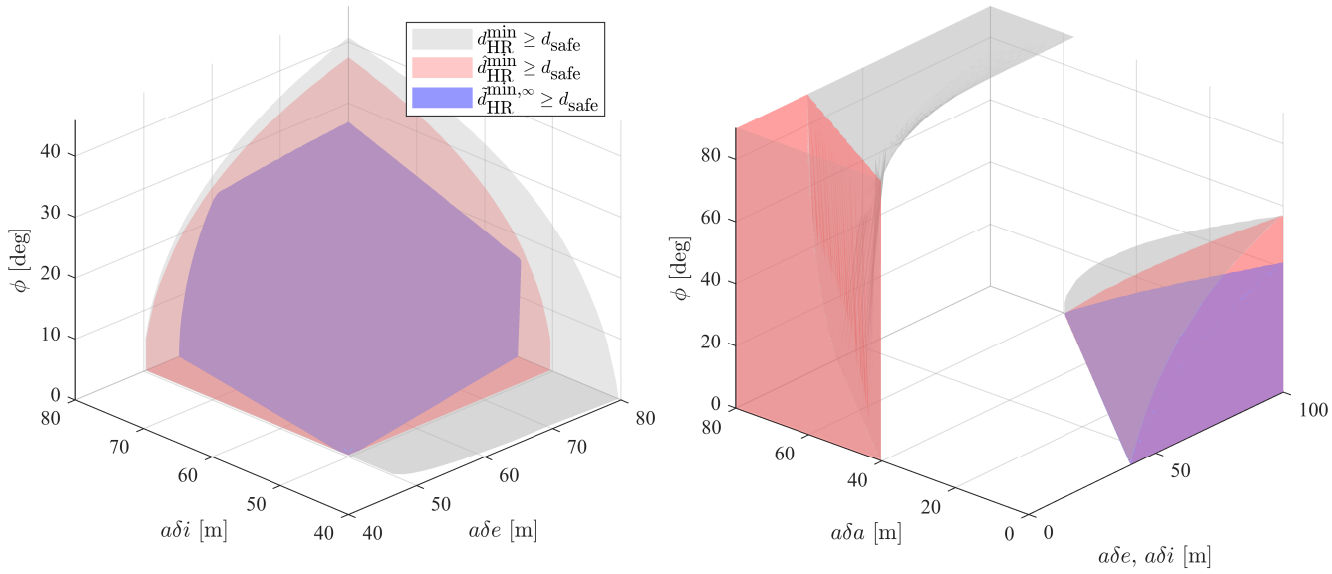

Fig. 4 Illustration of the different passive safety constraint sets for $d_{\text{safe}} = 40$ m with $a\delta\mathbf{e} = a\delta e(\cos\phi, \sin\phi)$ m, $a\delta\mathbf{i} = a\delta i(1,0)$ m, and $a\delta\mathbf{w} = (1,0)$. Left: w.r.t. the phase and magnitudes of the relative E/I vectors with $a\delta a = 10$ m. Right: w.r.t. relative semi-major axis and the phase and magnitudes of the relative E/I vectors but with $\delta e = \delta i$.

3 Robust Model Predictive Control

3.1 Problem Formulation

Consider the discrete-time linear time-varying (LTV) system

$$x_{t+1} = A_t x_t + B_t u_t + d_t + w_t, \tag{32}$$

for $t \in \mathbb{N}$, where $x_t \in \mathbb{R}^{n_\text{x}}$ are the n_x state variables at time t, $u_t \in \mathbb{R}^{n_\text{u}}$ are the n_u control variables at time t, and $d_t \in \mathbb{W}_t \subset \mathbb{R}^{n_\text{x}}$ and $w_t \in \mathbb{W}_t \subset \mathbb{R}^{n_\text{x}}$ are, respectively, known and unknown additive disturbances. The control objective is to drive the state x from an initial condition x_0 to a terminal set $\mathbb{X}_N \subset \mathbb{R}^{n_\text{x}}$ at most by time $t = N > 0$, i.e., ensuring

$$x_N \in \mathbb{X}_N, \tag{33}$$

while satisfying a set of path constraints

$$(x_t, u_t) \in \mathbb{C}_t, \quad \forall t \in \mathbb{N}_{[0,N-1]} \tag{34}$$

where $\mathbb{C}_t \subseteq \mathbb{R}^{n_\text{x}} \times \mathbb{R}^{n_\text{u}}$, and with a minimum-fuel trajectory, quantified by the control ℓ_1-norm

$$V(\mathbf{u}) \coloneqq \sum_{t=0}^{N-1} \|u_t\|_1 \tag{35}$$

with $\mathbf{u} \coloneqq (u_0, \ldots, u_{N-1})$.

Assumption 1. The disturbance w_t is bounded, zonotopic, and has zero mean, i.e.

$$\mathbb{W}_t = \left\{ G_t \xi_t : \xi_t \in \mathcal{B}_\infty^{n_\text{w}} \right\}, \quad \forall t \in \mathbb{N}_{[0,N-1]}, \tag{36}$$

with $G_t \in \mathbb{R}^{n_\text{x} \times n_\text{w}}$.

Assumption 2. The system parameters A_t, B_t, d_t, G_t for all $t \in \mathbb{N}_{[0,N-1]}$ are known offline, and at any time $t \in \mathbb{N}_{[0,N]}$ the current state x_t is known.

Assumption 3. The path and terminal constraint sets are non-empty, closed, convex, and polytopic, i.e., representable as

$$\begin{aligned} \mathbb{C}_t &= \{\gamma \in \mathbb{R}^{n_\mathrm{x}+n_\mathrm{u}} : C_t\gamma \leq b_t\}, \quad \forall t \in \mathbb{N}_{[0,N-1]} \\ \mathbb{X}_N &= \{x \in \mathbb{R}^{n_\mathrm{x}} : C_N x \leq b_N\}, \end{aligned} \tag{37}$$

where $C_t \in \mathbb{R}^{m_t \times (n_\mathrm{x}+n_\mathrm{u})}$, $b_t \in \mathbb{R}^{m_t}$ for $t \in \mathbb{N}_{[0,N-1]}$, and $C_N \in \mathbb{R}^{m_N \times n_\mathrm{x}}$, $b_N \in \mathbb{R}^{m_N}$, and m_t is the number of linear inequalities for the constraints at time t.

3.2 Robust MPC

Since the system is disturbed by the unknown, but bounded, disturbances $\mathbf{w} \coloneqq (w_0, \ldots, w_{N-1})$, the state evolution $\mathbf{x} \coloneqq (x_0, \ldots, x_N)$ cannot be exactly predicted. Therefore, the minimization of the cost (35) and the satisfaction of the constraints (33) and (34) must be performed by evaluating the worst-case realization of $\mathbf{w}$. The ideal Robust MPC can then be formulated as a minimax problem with robust constraints and optimized over a control policy $\boldsymbol{\pi}(\mathbf{x}) \coloneqq (\pi_0(\mathbf{x}), \ldots, \pi_{N-1}(\mathbf{x}))$ with $\pi_t(\cdot) : \Pi_t \to \mathbb{R}^{n_u}$ where $\Pi_t \subset \mathbb{R}^{Nn_\mathrm{x}}$ denotes the set of causal control policies at time t [1, Ch.3]. Thus yields Problem 1, for which we define $\mathbb{W} \coloneqq \mathbb{W}_0 \times \cdots \times \mathbb{W}_{N-1}$, and where $\mathbf{x}$ and its dependency on $\mathbf{w}$ is implicitly given by propagating (32) with the known initial condition x_0 and applying the control policy $u_t = \pi_t(\mathbf{x})$.

Problem 1 (*Minimax Robust MPC*)**.**

$$\min_{\boldsymbol{\pi}} \quad \max_{\mathbf{w}\in\mathbb{W}} V(\boldsymbol{\pi}(\mathbf{x})) \tag{38a}$$

$$\text{s.t.} \quad (x_t, \pi_t(\mathbf{x})) \in \mathbb{C}_t, \qquad \forall t \in \mathbb{N}_{[0,N-1]}, \mathbf{w} \in \mathbb{W} \tag{38b}$$

$$x_N \in \mathbb{X}_N, \qquad \forall \mathbf{w} \in \mathbb{W} \tag{38c}$$

Problem 1 is infinite-dimensional, since it optimizes over the function $\boldsymbol{\pi}$, and is therefore generally computationally intractable, especially for online deployment. To simplify the problem, a Tube-Based MPC approach can be taken [1, Ch.3], where the control policy $\boldsymbol{\pi}$ is parametrized in terms of a nominal/feedforward control profile $\mathbf{v} = (v_0, \ldots, v_{N-1})$ where $v_t \in \mathbb{R}^{n_\mathrm{u}}$ with its respective nominal state trajectory $\mathbf{z} = (z_0, \ldots, z_N)$, and a feedback term on the control tracking error $e_t \coloneqq x_t - z_t$ with gains $K_t \in \mathbb{R}^{n_\mathrm{u} \times n_\mathrm{x}}$, known as the *ancillary controller*, yielding

$$\pi_t(\mathbf{x}) = v_t + K_t e_t, \quad \forall t \in \mathbb{N}_{[1,N-1]} \tag{39}$$

with $u_0 = v_0$, and where $\mathbf{z}$ is obtained by propagating the unperturbed ($\xi_t = 0$) system model (32) for the nominal control $\mathbf{v}$

$$z_{t+1} = A_t z_t + B_t v_t + d_t, \quad z_0 \coloneqq x_0. \tag{40}$$

Problem (38) is now optimized over $\mathbf{v}$ and $(K_0, \ldots, K_{N-1})$ and thus has a finite-dimensional search space; it is, however, highly non-convex in K_t due to the bilinear terms with e_t in (39), which further compound through the propagation of the dynamic model. Therefore, further simplifications are typically employed to enable a computationally tractable deployment. For this reason, the ancillary gains K_t are often determined offline in practical Tube-Based Robust MPC applications, and the only decision variable becomes $\mathbf{v}$, yielding a convex problem at the cost of optimality, performance, and feasibility.

3.3 Linear Tube-Based MPC

Fixing the ancillary gains K_t in (39) enables a significant simplification of Problem 1, such that the complexity of the resulting optimization problem can be made equivalent to that of a non-robust linear MPC.

3.3.1 Constraint Tightening

We now seek to express the robust constraints (38b) and (38c) in closed-form with respect to $(\mathbf{z}, \mathbf{v})$. Using Assumptions 1 and 3, the robust constraints (38b) can be equivalently expressed as

$$\max_{\boldsymbol{\xi}_{t-1} \in \mathcal{B}_\infty^{tn_\mathrm{w}}} c_{t,i}^\mathrm{T}(x_t, u_t) \leq b_{t,i}, \quad \forall t \in \mathbb{N}_{[1,N-1]},\, i \in \mathbb{N}_{[1,m_t]}, \tag{41}$$

where $\boldsymbol{\xi}_{t-1} \coloneqq (\xi_0, \ldots, \xi_{t-1})$. For the control policy (39), the perturbed states and controls (x_t, u_t) are given by

$$\begin{aligned} \begin{bmatrix} x_t \\ u_t \end{bmatrix} &= \begin{bmatrix} z_t \\ v_t \end{bmatrix} + \begin{bmatrix} G_t^\mathrm{x} \\ G_t^\mathrm{u} \end{bmatrix} \boldsymbol{\xi}_{t-1}, \quad \forall t \in \mathbb{N}_{[1,N-1]}, \\ x_N &= z_N + G_N^\mathrm{x} \boldsymbol{\xi}, \end{aligned} \tag{42}$$

with

$$\begin{aligned} G_{t+1}^\mathrm{x} &= \begin{bmatrix} (A_t + B_t K_t) G_t^\mathrm{x} & G_t \end{bmatrix} \\ G_t^\mathrm{u} &= K_t G_t^\mathrm{x} \end{aligned} \qquad \forall t \in \mathbb{N}_{[1,N-1]}, \tag{43}$$

with $G_1^\mathrm{x} \coloneqq G_0$. Applying the fact $\max_{\xi \in \mathcal{B}_\infty^n} \{c^\mathrm{T} \xi\} = \|c\|_1$ to (41) yields

$$C_t(z_t, v_t) \leq b_t - \beta_t, \quad \forall t \in \mathbb{N}_{[1,N-1]}, \tag{44}$$

where $\beta_t \coloneqq (\beta_{t,1}, \ldots, \beta_{t,m_t})$ are constraint tightening terms computed as

$$\beta_{t,i} \coloneqq \left\| c_{t,i}^\mathrm{T} \left(G_t^\mathrm{x}, G_t^\mathrm{u} \right) \right\|_1, \quad \forall t \in \mathbb{N}_{[1,N-1]},\, i \in \mathbb{N}_{[1,m_t]}. \tag{45}$$

Similarly, the robust terminal constraint (38c) becomes

$$C_N z_N \leq b_N - \beta_N, \tag{46}$$

where $\beta_N \coloneqq (\beta_{N,1}, \ldots, \beta_{N,m_N})$ with

$$\beta_{N,i} \coloneqq \left\| c_{N,i}^\mathrm{T} G_N^\mathrm{x} \right\|_1, \quad \forall i \in \mathbb{N}_{[1,m_N]}. \tag{47}$$

3.3.2 Cost Function

Regarding the robust cost function (38a), applying the control policy (39), yields

$$\max_{\mathbf{w} \in \mathbb{W}} V(\boldsymbol{\pi}(\mathbf{x})) = \max_{\boldsymbol{\xi} \in \mathcal{B}_\infty^{Nn_\mathrm{w}}} \sum_{t=0}^{N-1} \left\| v_k + G_t^\mathrm{u} \boldsymbol{\xi}_t \right\|_1. \tag{48}$$

Although this cost function is convex in $\mathbf{v}$ [39, §3.2.3], it cannot be expressed in closed-form without enumeration of the vertices of $\mathcal{B}_\infty^{Nn_\mathrm{w}}$, which would scale the problem dimensions exponentially with Nn_w and quickly lead to computational intractability. Therefore, we instead consider an upper-bound derived with the triangle inequality

$$\max_{\boldsymbol{\xi} \in \mathcal{B}_\infty^{Nn_\mathrm{w}}} \sum_{t=0}^{N-1} \left\| v_t + G_t^\mathrm{u} \boldsymbol{\xi}_t \right\|_1 \leq V(\mathbf{v}) + \max_{\boldsymbol{\xi} \in \mathcal{B}_\infty^{Nn_\mathrm{w}}} \sum_{t=0}^{N-1} \left\| G_t^\mathrm{u} \boldsymbol{\xi}_t \right\|_1. \tag{49}$$

Since the rightmost term is constant in $\mathbf{v}$, we can equivalently optimize just for $V(\mathbf{v})$.

The resulting full Linear Tube-Based MPC formulation in LP-representable form is presented in Problem 2.

Problem 2 (*LP-representable minimum fuel Linear Tube-Based MPC*)**.**

$$\min_{\mathbf{z},\mathbf{v}} \quad \sum_{t=0}^{N-1} \|v_t\|_1 \tag{50a}$$

$$\text{s.t.} \quad z_0 = x_0 \tag{50b}$$

$$z_{t+1} = A_t z_t + B_t v_t + d_t, \qquad \forall t \in \mathbb{N}_{[0,N-1]} \tag{50c}$$

$$C_t(z_t, v_t) \leq b_t - \beta_t, \qquad \forall t \in \mathbb{N}_{[0,N-1]} \tag{50d}$$

$$C_N z_N \leq b_N - \beta_N \tag{50e}$$

3.4 Shrinking-Horizon MPC

The default MPC approach uses the *receding-horizon* strategy [1], with which it is often synonymously identified (Receding Horizon Control), whereby the optimal control time-horizon slides forward at each subsequent control re-optimization, simply by virtue incrementing the time-step and maintaining the prediction horizon length. This strategy is suitable for stabilizing control problems, and follows naturally from the fact that an infinite-horizon optimal control problem is the ideal formulation, e.g., for stability, but is generally computationally intractable when state and control constraints exist, such that a receding finite-horizon is the best practical alternative.

On the other hand, for problems with an economic objective function [1, §2.8], as opposed to a regulation or tracking objective, it is known that the receding-horizon strategy can lead to very slow convergence to the desired terminal setpoint, since the cost function does not encourage approaching it before the final time-step, which is continually delayed upon every recomputation. This is indeed the observed behaviour for the MPC formulation (50) [8], which is undesirable given that rendezvous manoeuvres must typically adhere to a pre-determined mission timeline [10]. Therefore, the use of the *shrinking-horizon* strategy has been proposed in the literature as an alternative, whereby the length of the prediction of horizon is *decremented* at every time-step, such that the end of the horizon remains at the same absolute time-instant [2, 8, 23, 24]. One downside in this strategy is that problem infeasibility is more likely, namely as the horizon length approaches 1 and the MPC can no longer arbitrarily manipulate the state with the remaining number of control actions; nonetheless, if robust/recursive feasibility is ensured, then finite-time completion is guaranteed, albeit at a pre-determined and rigid time.

4 System Level Synthesis Model Predictive Control

4.1 System Level Parametrization

System Level Synthesis (SLS) is a control synthesis framework for linear systems and linear time-varying (LTV) state-feedback controllers which leverages a special parameterization of the disturbed closed-loop system response that enables an exact convex re-formulation of the controller synthesis problem [12]. When applied to MPC, it can be interpreted as a fully equivalent re-parameterization of the propagated state and control variables for system (32) which recovers a convex search space for a parametrized linear control policy that generalizes (39). Therefore, it enables a better approximation of Problem 1 — the ideal Robust MPC formulation — with respect to the linear Tube-Based MPC Problem 2, and is thus expected to yield better optimality, closed-loop performance, and feasibility.

Consider a modification to the control policy $\mathbf{u} = \boldsymbol{\pi}(\cdot)$ in (39) to also include feedback terms on past tracking errors

$$u_t = \pi_t(\mathbf{x}) = v_t + \sum_{j=1}^{t} K_{t,j}(x_j - z_j), \quad \forall t \in \mathbb{N}_{[1,N-1]} \tag{51}$$

with $u_0 = v_0$. The additional degrees of freedom in $K_{t,j}$ for $j < t$ allow for performing a change of variables to a convex feasible space without any loss of generality. Namely, it can be shown that (51) is equivalently expressed as

$$u_t = v_t + \sum_{j=0}^{t-1} \Phi^{\mathrm{u}}_{t,j} w_j, \quad \forall t \in \mathbb{N}_{[0,N-1]} \tag{52}$$

where $\Phi^{\mathrm{u}}_{t,j} \in \mathbb{R}^{n_{\mathrm{u}} \times n_{\mathrm{x}}}$ can be interpreted as the system response for the control u at time t to the disturbance w at time j. Applying (52) to (32), the state can similarly be shown to be expressed as

$$x_t = z_t + \sum_{j=0}^{t-1} \Phi^{\mathrm{x}}_{t,j} w_j, \tag{53}$$

where $\Phi^{\mathrm{x}}_{t,j} \in \mathbb{R}^{n_{\mathrm{x}} \times n_{\mathrm{x}}}$ is the system response for the state x at time t to the disturbance w at time j, given by

$$\begin{aligned} \Phi^{\mathrm{x}}_{t+1,t} &= I_{n_{\mathrm{x}}}, \quad \forall t \in \mathbb{N}_{[0,N-1]} \\ \Phi^{\mathrm{x}}_{t+1,j} &= A_t \Phi^{\mathrm{x}}_{t,j} + B_t \Phi^{\mathrm{u}}_{t,j}, \quad \forall t \in \mathbb{N}_{[1,N-1]},\ j \in \mathbb{N}_{[0,t-1]} \end{aligned} \tag{54}$$

which is analogous to the dynamic equations (40) for the nominal trajectory. Therefore, rather than optimizing over the gains $K_{t,j}$ in a non-convex feasible space, we can optimize over the system responses $(\Phi^{\mathrm{x}}_{t,j}, \Phi^{\mathrm{u}}_{t,j})$, which are subject to the affine subspace (54) and provide the affine expressions (52) and (53) for the perturbed state and control variables (x_t, u_t), thus yielding a convex feasible space.

Given system responses $(\Phi^{\mathrm{x}}_{t,j}, \Phi^{\mathrm{u}}_{t,j})$ satisfying (54), the respective gains $K_{t,j}$ in (51) that they parametrize can be computed with [12]

$$\begin{bmatrix} K_{1,1} & & \\ \vdots & \ddots & \\ K_{N-1,1} & \cdots & K_{N-1,N-1} \end{bmatrix} = \begin{bmatrix} \Phi^{\mathrm{u}}_{1,0} & & \\ \vdots & \ddots & \\ \Phi^{\mathrm{u}}_{N-1,0} & \cdots & \Phi^{\mathrm{u}}_{N-1,N-2} \end{bmatrix} \begin{bmatrix} \Phi^{\mathrm{x}}_{1,0} & & \\ \vdots & \ddots & \\ \Phi^{\mathrm{x}}_{N-1,0} & \cdots & \Phi^{\mathrm{x}}_{N-1,N-2} \end{bmatrix}^{-1} \tag{55}$$

Remark 5. See [12] for the formal proof of equivalence of $(\Phi^{\mathrm{x}}_{t,j}, \Phi^{\mathrm{u}}_{t,j})$ with $K_{t,j}$. We highlight, however, some differences in the present formulation with respect to that presented in [12], which are adopted from [20]: 1) different convention for the indices of the system responses, that is more intuitive to us; 2) rather than optimizing over system responses to the initial condition, we equivalently optimize over the nominal trajectory $(\mathbf{z}, \mathbf{v})$, which removes redundant optimization variables (that would otherwise have a non-unique solution) and better resembles the typical form of Tube-Based MPC.

4.2 Robust Constraints

Given the system level parametrization $(\Phi^{\mathrm{x}}_{t,j}, \Phi^{\mathrm{u}}_{t,j})$, we now proceed to formulate the robust constraints (38b) and (38c) in closed-form. Substituting x_t and u_t with (52) and (53) yields

$$C_t \left(\gamma_t + \sum_{j=0}^{t-1} \Phi_{t,j} w_j \right) \leq b_t, \quad \forall \mathbf{w} \in \mathbb{W},\ t \in \mathbb{N}_{[1,N]}, \tag{56}$$

where $\gamma_t \coloneqq (x_t, u_t)$, $\forall t \in \mathbb{N}_{[0,N-1]}$, $\Phi_{t,j} \coloneqq (\Phi^x_{t,j}, \Phi^u_{t,j})$, $\forall t \in \mathbb{N}_{[0,N-1]}$, $\forall t \in \mathbb{N}_{[1,N-1]}$, $j \in \mathbb{N}_{[0,t-1]}$, and for $t = N$ we have $\gamma_N \coloneqq z_N$ and $\Phi_{N,j} \coloneqq \Phi^{\mathrm{x}}_{N,j}$, $\forall j \in \mathbb{N}_{[0,N-1]}$. We can evaluate the worst-case of the left-hand side independently for each $w_j = G_j\xi_j$, yielding the equivalent constraints

$$c_{t,i}^T\gamma_t + \sum_{j=0}^{t-1} \max_{\xi_j \in \mathcal{B}_\infty^{n_{\mathrm{w}}}} c_{t,i}^T \Phi_{t,j} G_j \xi_j \leq b_{t,i}, \quad \forall t \in \mathbb{N}_{[1,N]},\ i \in \mathbb{N}_{[1,m_t]}, \tag{57}$$

where $(c_{t,1}^T, \ldots, c_{t,m_t}^T) = C_t$ and $(b_{t,1}, \ldots, b_{t,m_t}) = b_t$. Since $\max_{\xi \in \mathcal{B}_\infty^n}\{c^T\xi\} = \|c\|_1$, the robust constraints become

$$c_{t,i}^T\gamma_t + \sum_{j=0}^{t-1} \|c_{t,i}^T \Phi_{t,j} G_j\|_1 \leq b_{t,i}, \quad \forall t \in \mathbb{N}_{[1,N]},\ i \in \mathbb{N}_{[1,m_t]}, \tag{58}$$

which are convex and polyhedral, and thus linearly representable. The path constraint $C_0\gamma_0 \leq b_0$ is not robustified since x_0 and u_0 are assumed to be known exactly.

4.3 Robust Objective

Similarly, we now attempt formulate the robust objective (38a) in closed-form using the modified control policy (51), re-parametrized with $\mathbf{\Phi}$. We have

$$\max_{\mathbf{w} \in \mathbb{W}} V(\boldsymbol{\pi}(\mathbf{x})) = \|v_0\|_1 + \max_{\mathbf{w} \in \mathbb{W}} \sum_{t=1}^{N-1} \left\| v_t + \sum_{j=0}^{t-1} \Phi^{\mathrm{u}}_{t,j} w_j \right\|_1, \tag{59}$$

which, as in (48), cannot be reformulated with a simple closed-form expression without vertex enumeration, which would result in exponential problem complexity in Nn_{w}. To avoid this intractable complexity, a simpler upper-bound is provided in the following result.

Proposition 4. *The robust objective function* (59) *is upper-bounded by*

$$\max_{\mathbf{w} \in \mathbb{W}} V(\boldsymbol{\pi}(\mathbf{x})) \leq V(\mathbf{v}) + \sum_{t=1}^{N-1} \sum_{j=0}^{t-1} \left\| \Phi^{\mathrm{u}}_{t,j} G_j \right\|_{1,1}. \tag{60}$$

Proof. Similarly to (49), apply the triangle inequality to all terms within the ℓ_1-norm in (59) and use the fact that $\mathbf{v}$ is independent of the disturbance, yielding

$$(59) \leq V(\mathbf{v}) + \max_{\boldsymbol{\xi} \in \mathcal{B}_\infty^{Nn_{\mathrm{w}}}} \sum_{t=1}^{N-1} \sum_{j=0}^{t-1} \left\| \Phi^{\mathrm{u}}_{t,j} G_j \xi_j \right\|_1. \tag{61}$$

An upper-bound for the maximum in (61) can be obtained by taking the maximum of each term in the sum independently, yielding $\sum_{t=1}^{N-1}\sum_{j=0}^{t-1}\sum_{i=1}^{n_{\mathrm{u}}} \max_{\boldsymbol{\xi} \in \mathcal{B}_\infty^{Nn_{\mathrm{w}}}} \left| e_i^{\mathrm{T}} \Phi^{\mathrm{u}}_{t,j} G_j \xi_j \right|$. Using $\max_{\xi \in \mathcal{B}_\infty^n}\{c^T\xi\} = \|c\|_1$, it becomes $\sum_{t=1}^{N-1}\sum_{j=0}^{t-1}\sum_{i=1}^{n_{\mathrm{u}}} \left\| e_i^{\mathrm{T}} \Phi^{\mathrm{u}}_{t,j} G_j \right\|_1$. Using the definition of $\|\cdot\|_{1,1}$ completes the proof. □

Optimizing the upper-bound (60) rather than the original cost (59) yields an approximate problem that is LP-representable with a polynomial number of auxiliary variables and constraints, at the cost of some optimality. Furthermore, notice that this result is similar to (49), but now the corresponding cost due to the disturbances is no longer constant in the decision variables, meaning that SLS-MPC has greater flexibility to impact its own fuel performance by better predicting its closed-loop behaviour. The full SLS-MPC problem in LP-representable form is presented in Problem 3.

Problem 3 (*LP-representable minimum fuel SLS-MPC*)**.**

$$\min_{\substack{\mathbf{z},\mathbf{v}\\ \boldsymbol{\Phi}^{\mathrm{x}},\boldsymbol{\Phi}^{\mathrm{u}}}} \quad \|v_0\|_1 + \sum_{t=1}^{N-1}\left(\|v_t\|_1 + \sum_{j=0}^{t-1}\left\|\Phi^{\mathrm{u}}_{t,j}G_j\right\|_{1,1}\right) \tag{62a}$$

$$\text{s.t.} \quad z_0 = x_0 \tag{62b}$$

$$z_{t+1} = A_t z_t + B_t v_t + d_t, \qquad \forall t \in \mathbb{N}_{[0,N-1]} \tag{62c}$$

$$\Phi^{\mathrm{x}}_{t+1,t} = I_{n_{\mathrm{x}}}, \qquad \forall t \in \mathbb{N}_{[0,N-1]} \tag{62d}$$

$$\Phi^{\mathrm{x}}_{t+1,j} = A_t\Phi^{\mathrm{x}}_{t,j} + B_t\Phi^{\mathrm{u}}_{t,j}, \qquad \forall t \in \mathbb{N}_{[1,N-1]},\ j \in \mathbb{N}_{[0,t-1]} \tag{62e}$$

$$C_0(z_0, v_0) \leq b_0 \tag{62f}$$

$$c^T_{t,i}(z_t, v_t) + \sum_{j=0}^{t-1}\left\|c^T_{t,i}\left(\Phi^{\mathrm{x}}_{t,j}, \Phi^{\mathrm{u}}_{t,j}\right)G_j\right\|_1 \leq b_{t,i}, \qquad \forall t \in \mathbb{N}_{[1,N-1]},\ i \in \mathbb{N}_{[1,m_t]} \tag{62g}$$

$$c^T_{N,i}z_N + \sum_{j=0}^{N-1}\left\|c^T_{N,i}\Phi^{\mathrm{x}}_{N,j}G_j\right\|_1 \leq b_{N,i}, \qquad \forall i \in \mathbb{N}_{[1,m_N]} \tag{62h}$$

4.4 One-Shot SLS-MPC for Rendezvous

The greatest downside of MPC is the computational demand of solving the respective optimization problem, which can be particularly challenging for a rendezvous application due to the limited computational power available for a radiation hardened onboard computer (OBC). Another potentially significant downside is the lack of a guarantee that a solution — or even just a feasible point — will be found by the numerical optimizer within the allotted timeslot, which can be particularly detrimental to a rendezvous application due to its inherent safety-critical nature. Furthermore, these limitations are amplified for SLS-MPC with respect to linear Tube-Based MPC, given that the dimensions of the matrix decision variables ($\boldsymbol{\Phi}^{\mathrm{x}}, \boldsymbol{\Phi}^{\mathrm{u}}$) and respective constraints in Problem 3 scale quadratically with the system dimensions and prediction horizon length, and thus the problem has significantly greater computational complexity. Nonetheless, we propose a strategy that leverages the strengths of SLS-MPC and the particularities of a typical rendezvous approach to limit the effect of these downsides and potentially enable MPC with respect to the above-mentioned downsides, namely in terms of reducing its dependency on recursive real-time optimization, despite its greater computational demand.

Indeed, a typical rendezvous approach is comprised of a sequence of separate manoeuvres performed between *hold points* of shortening relative distances that are designed offline [10]. The SLS-MPC Problem 3 can thus be modelled to consider the *full* transfer manoeuvre between two such hold points, optimizing a nominal trajectory ($\mathbf{z}, \mathbf{v}$) and the system responses ($\boldsymbol{\Phi}^{\mathrm{x}}, \boldsymbol{\Phi}^{\mathrm{u}}$) that ensure robust constraint satisfaction. The system responses equivalently parametrize a linear controller $\mathbf{K}$ which, for the present rendezvous problem, encodes a guidance/control policy for trajectory correction. Therefore, if the SLS-MPC problem is successfully solved just once, this policy becomes available as a backup solution that guarantees the safe attainment of the next hold point, despite the uncertainty and disturbances considered, without any further re-optimizations.

Regarding the initial SLS-MPC optimization for each manoeuvre, we can leverage the fact that, in typical rendezvous operations, the chaser S/C may maintain the hold points in-between manoeuvres for a flexible amount of time, typically to synchronise the mission timeline, commission sensors, perform ground monitoring, etc. [10]. Therefore, the first optimization may be performed while safely maintaining the time-flexible hold point, and thus without hard real-time computation requirements. If successful, this initially computed manoeuvre and correction policy are guaranteed to achieve the next hold point with robust performance guarantees and without any re-optimizations. Notably, this approach is equivalent

to a *shrinking-horizon* strategy, rather than the *receding-horizon* standard in MPC, but, as discussed in Section 3.4, the former can indeed be better suited for the present rendezvous problem. Mid-course re-optimizations are still available, as in a typical MPC, but these also have no hard real-time requirements since a feasible backup solution is available and thus are solely necessary for improving fuel-performance, rather than being required to ensure safety or terminal manoeuvre accuracy.

In summary, the proposed strategy is based on four main points:

1) The prediction horizon covers a full transfer manoeuvre between two hold points;
2) A shrinking-horizon strategy ensures the maximum manoeuvre duration allowed;
3) The first optimization is performed while maintaining a safe and time-flexible hold point;
4) The first optimal trajectory and correction policy are available as a feasible and safe backup.

In addition, to further improve computational tractability, the SLS-MPC problem can indeed be solved just once per manoeuvre at the cost of optimality, in what we refer to as *One-Shot SLS-MPC* (OS-SLS), whereby the optimized system responses $(\mathbf{\Phi}^{\mathrm{x}}, \mathbf{\Phi}^{\mathrm{u}})$ are converted to gains $\mathbf{K}$ using (55), which are then used to close the loop and perform the full manoeuvre until completion.

As a third alternative that is a computational middle ground between full closed-loop SLS-MPC and OS-SLS-MPC, MPC re-computations may optimize solely over the nominal trajectory $(\mathbf{z}, \mathbf{v})$ and re-use the initially computed system responses $(\mathbf{\Phi}^{\mathrm{x}}, \mathbf{\Phi}^{\mathrm{u}})$, which we refer to as *Nominal-Replan SLS-MPC* (NR-SLS-MPC). This approach yields an optimization problem similar and computationally equivalent to the linear Tube-Based MPC Problem 2, but where the constraint tightening terms $\beta_{k,i}$ are computed online by the first SLS-MPC optimization rather than offline, thus potentially yielding better performance and feasibility.

Remark 6. The idea of relying on a backup control policy to reduce the critical dependency on real-time optimization, or to avoid mid-course optimizations altogether, is also applicable to the Linear Tube-Based MPC approach of Section 3.3, via the ancillary controller. This policy, however, is determined offline and not usually designed for use on the real plant, but rather to approximate the MPC closed-loop action within the MPC dynamic model itself and reduce the conservativeness of the robust constraint tightening, and would thus not necessarily yield good practical performance if used instead of the MPC itself. In contrast, SLS-MPC optimizes the feedback law online for the specific initial conditions provided and considering the actual MPC objective and constraints desired, and thus may perform sufficiently well by itself, within the limitations of the structure of the feedback law, namely linearity. At worst, the SLS-MPC methodology proposed here can be utilized for the offline design of improved ancillary controllers to use with existing Tube-Based MPC formulations.

5 Numerical Results

We next present Monte-Carlo simulation results for a low Earth orbit (LEO) rendezvous transfer manoeuvre at far-range to demonstrate the SLS-MPC formulations proposed in Section 4, as well as the simpler Linear Tube-Based MPC formulation presented in Section 3.3 for comparison. The relevant simulation and MPC parameters are presented in Table 1. Both the simulation model and the MPC prediction model consider the linearised ROE model with J_2 and drag presented in Section 2.2, but the latter has a greater sampling period. The simulation includes the uniform-distributed additive disturbance w_t in (32) with $G_t = \gamma_{\mathrm{w}}\mathbf{B}(\cdot)$, where $\mathbf{B}$ is the input matrix in (13) and γ_{w} is the magnitude of the disturbance acceleration; the fact that the disturbance is aligned with the input matrix and sampled at MPC frequency is unrealistic, namely in that it limits the reachability of the disturbances, but is assumed for the sake of simplicity of the simulation environment. To improve numerical conditioning for the optimizer, the optimization problems consider a dimensionalized ROE state, i.e., $x = a\delta\boldsymbol{\alpha}$. The MPC considers the passive safety constraint (29) as a path constraint, as well as the path constraint

Parameter	Value
Target semi-major axis (a)	6878 km
Target eccentricity (e)	0.01
Initial target angular orbital elements (i, Ω, ω, M)	(55,75,125,0) deg
Standard gravitational parameter (μ)	3.986004418×10^{14} m^3/s^2
Geopotential second order zonal coefficient (J_2)	$1.08262982131\times10^{-3}$
Relative inverse ballistic coefficient (δB)	-0.015 m^2/kg
Density model (ρ)	NRLMSISE-00
Earth angular velocity (ω_{Earth})	7.2921159×10^{-5} rad/s
Initial relative state ($a\delta\boldsymbol{\alpha}_0$ or x_0)	(0,1000,0,100,0,100) m
Desired relative state ($a\delta\boldsymbol{\alpha}_{\text{f}}$)	(0,100,0,50,0,50) m
Final state tolerance ($a\delta\boldsymbol{\alpha}_{\text{tol}}$)	(5, 20, 5, 5, 5, 5) m
Maximum control/ΔV ($\delta v_{\max}$)	0.01 m/s
Minimum passive safety distance (d_{safe})	40 m
Maximum disturbance acceleration magnitude (γ_{w})	1 (Sec. 5.1) and 1.5 (Sec. 5.2) µm/s^2
Manoeuvre duration (T)	4.76 h (3 orbital periods)
MPC prediction horizon (N)	15
MPC sampling period (T/N)	1135 s
MPC optimizer	MOSEK (default options), parsed with CVX
Simulation sampling period (Δt)	22.7 s
Monte-Carlo simulations	100
CPU	Intel i7-8565U

Table 1 Simulation and MPC parameters.

$\|u_t\|_\infty \leq \delta v_{\max}\ \forall t \in \mathbb{N}_{[0,N-1]}$ to ensure a maximum ΔV at each time-step. The manoeuvre accuracy requirement is defined as a terminal box constraint about the nominal desired ROE state $\delta\boldsymbol{\alpha}_{\text{f}}$ with a tolerance $\delta\boldsymbol{\alpha}_{\text{tol}}$, i.e., $\mathbb{C}_{\text{f}} = \{x \in \mathbb{R}^{n_{\text{x}}} : |x - a\delta\boldsymbol{\alpha}_{\text{f}}| \leq a\delta\boldsymbol{\alpha}_{\text{tol}}\}$.

We test and compare three MPC formulations:

1) Linear Tube-Based MPC (LTB-MPC): Problem 2 with Shrinking-Horizon strategy (Sec. 3.4);
2) System Level Synthesis MPC (SLS-MPC): Problem 3 with Shrinking-Horizon strategy;
3) One-Shot SLS-MPC (OS-SLS-MPC): Problem 3 with the strategy proposed in Section 4.4.

We present two different Monte-Carlo simulation campaign. The first considers a smaller disturbance acceleration magnitude and is used to compare LTB-MPC and SLS-MPC in terms of fuel performance and computation time. The second campaign considers a 50% greater disturbance magnitude — for which LTB-MPC yields an infeasible optimization problem — and compares SLS-MPC and OS-SLS-MPC.

5.1 Scenario 1

In this first Monte-Carlo simulation, we consider a disturbance acceleration magnitude of $\gamma_{\text{w}} = 1$µm/s^2, and we compare the performance of LTB-MPC and SLS-MPC. The ancillary controller K_t in (39) of the former, used for robustly tightening the constraints as in Section 3.3.1, is given by the discrete-time finite-horizon time-varying linear quadratic regulator (LQR) with the same horizon N and prediction model as the MPC, the state and control stage cost matrices $Q = 0.1\mathbf{I}_{n_{\text{x}}}$ and $R = \mathbf{I}_{n_{\text{u}}}$, and terminal state cost $Q_{\text{f}} = 10\mathbf{I}_{n_{\text{x}}}$.

Figure 5 plots the ROE states with respect to time, highlighting the simulation for the nominal case ($w = 0$) and the trajectory dispersions for the simulations with the random additive disturbances, showing similar but different nominal trajectories and dispersions, showing that the terminal accuracy requirement

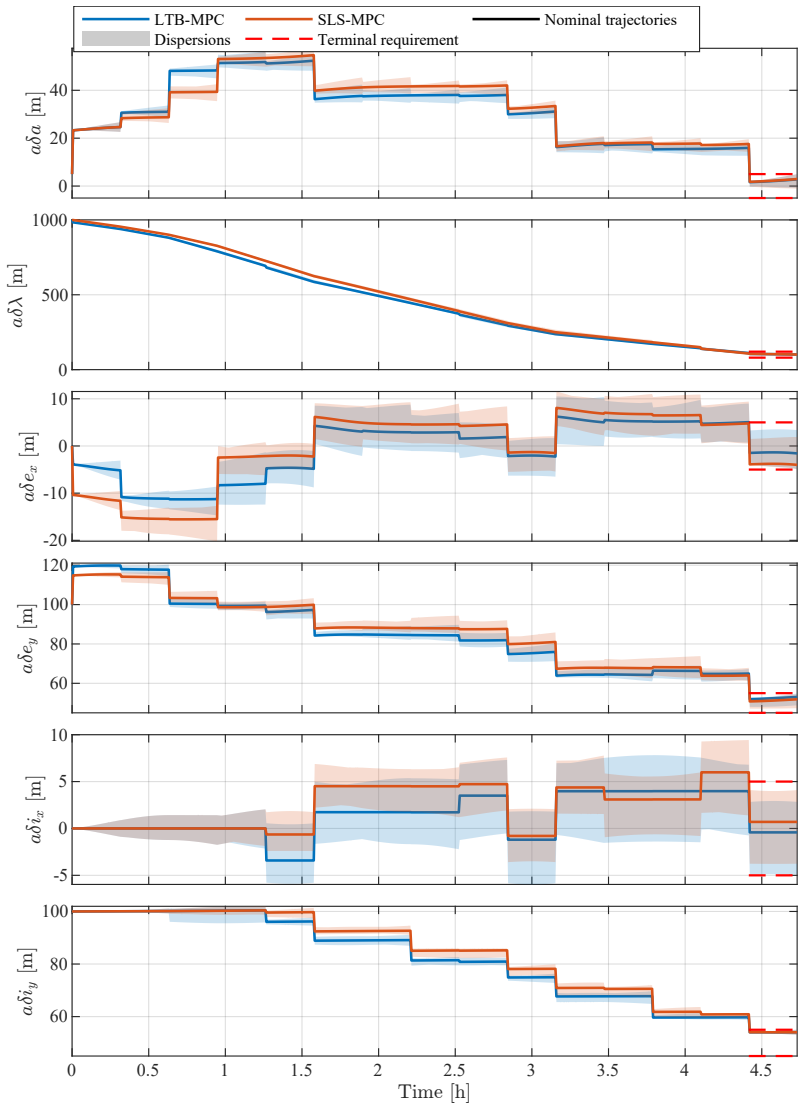

Fig. 5 Time-evolution of the ROE trajectories for each controller in Monte-Carlo simulation.

is robustly satisfied in all cases. The sudden and periodic shrinking of the dispersion intervals corresponds to the MPC re-computation time-instants, at which an updated ΔV is computed and instantly applied, reducing the dispersions to ensure constraint satisfaction.

Figure 6 shows the same trajectories but expressed in LVLH position, namely in the V-bar/R-bar and H-bar/R-bar planes, showing similar trajectories that start from the initial hold point $\delta\boldsymbol{\alpha}_0$ to the final one $\delta\boldsymbol{\alpha}_\mathrm{f}$, which describe ellipses in LVLH. We highlight the ROE passive safety concept described in Section 2.4, whereby the relative trajectories are also elliptical, circling the V-bar axis while travelling along it, such that the free-drift trajectories resulting from the loss of control does not result in a collision with the target S/C. This concept is also illustrated in Figure 7, which plots the minimum H-bar/R-bar distance along one orbit $d_{\mathrm{HR}}^{\min}$ with respect to time, showing that, according to this metric, passive safety is maintained throughout the whole trajectory. Furthermore, we highlight that the metric plotted is that from (19), computed as in reference [29] via the roots of a fourth-order polynomial, rather than its convex and polyhedral relaxation derived in Section 2.4.3 and used in the MPC path constraints; nonetheless, Figure 7 shows that the original metric closely approaches the constraint boundary of 40 meters, showing that — in light of the discussion in Remark 4 — the constraint (29) can have low conservativeness, partly due to the initial and final hold points being designed with parallel relative E/I vectors.

Finally, Figure 8 plots the ΔV commands for each controller. The first observation is that, in nominal conditions, the control profile is quite sparse, which is expected behaviour when minimizing a

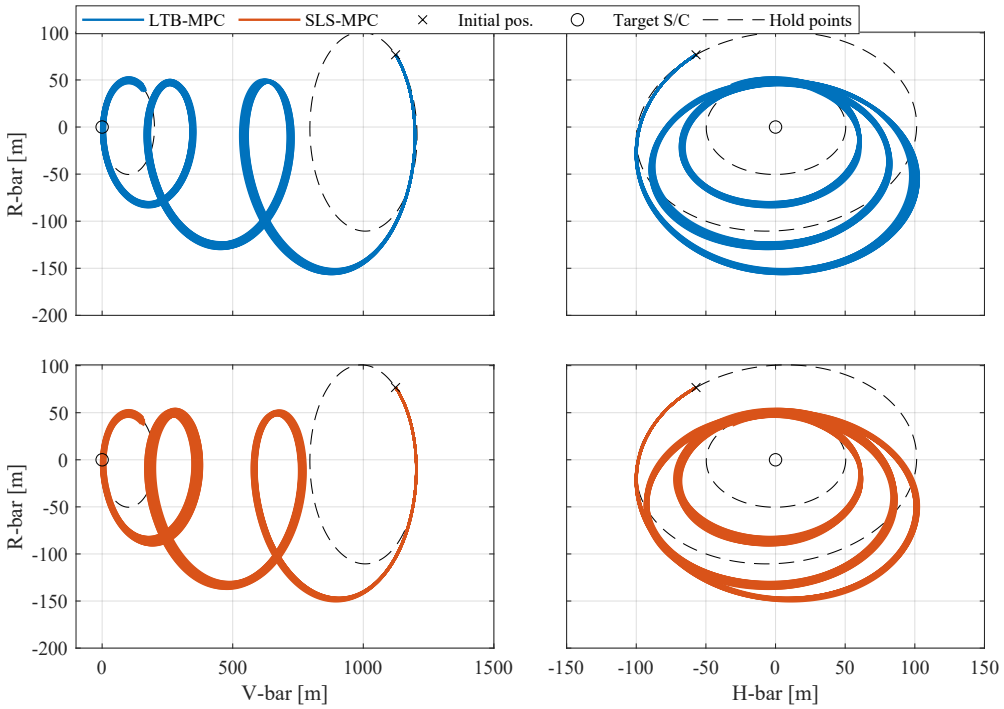

Fig. 6 Time-evolution of the LVLH trajectories for each controller in Monte-Carlo simulation.

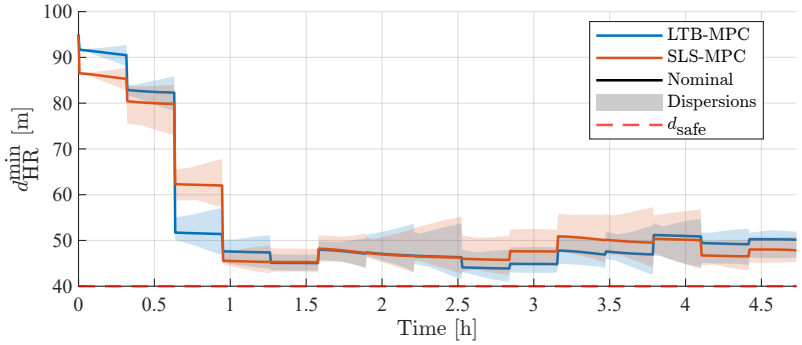

Fig. 7 Time-evolution of the minimum distance along H-bar/R-bar ($d_{\mathbf{HR}}^{\mathbf{min}}$ from eq. (19)) for each controller in Monte-Carlo simulation.

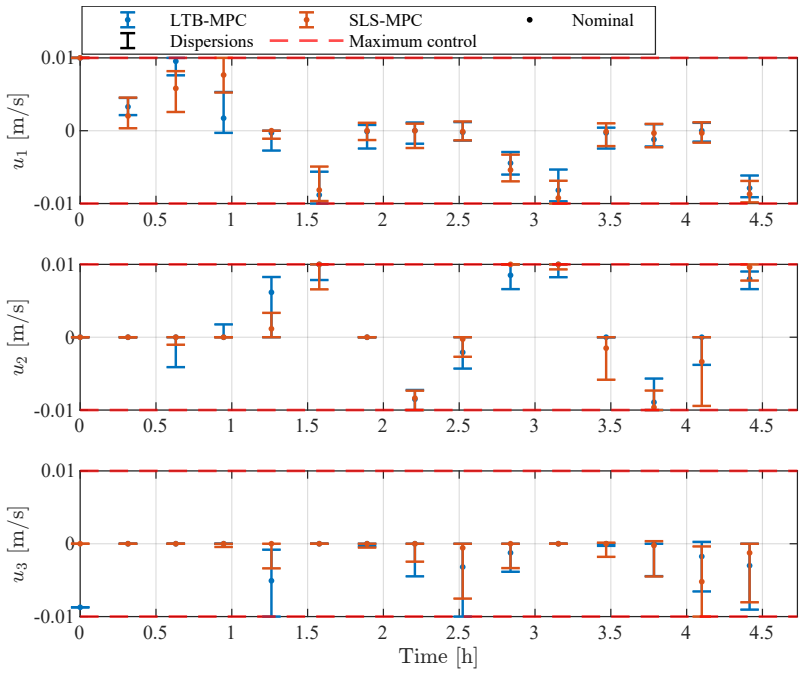

Fig. 8 Time-evolution of the control variables commanded by each controller in Monte-Carlo simulation.

norm cost function like (35), while the presence of disturbances demands additional correction ΔVs to ensure constraint satisfaction. Although the control profiles of the two controllers are different, it is not readily apparent which is most efficient. Table 2 presents metrics on the total commanded ΔV for each controller, showing that SLS-MPC has better performance in terms of the nominal case, the mean, and the worst-case across the Monte-Carlo simulations, although the difference is small (≈8% mean reduction). This improvement in performance is due to the fact that SLS-MPC can explicitly, albeit conservatively, optimize for the ΔV cost of trajectory corrections, namely the rightmost term in (62a), by optimizing the control policy $\mathbf{K}$, whereas for LTB-MPC the equivalent cost term in (49) becomes independent of the decision variables to ensure a tractable cost function, becoming dependent only on the offline-determined ancillary controller. This improvement comes at the cost of increased computational demand: for the first optimization problem in the simulation, which has the longest prediction horizon due to the Shrinking-Horizon, LTB-MPC has a computation time in the order of 10 ms whereas SLS-MPC has a computation time in the order of 4 s.

Table 2 also shows the fuel performance of OS-SLS-MPC, despite its results not being presented for the previous figures to avoid overburdening them; the results show that OS-SLS-MPC has a cost greater than LTB-MPC, namely ≈6% on average, which is a relatively small increase given that, as discussed in Section 4.4, the latter is dependent on real-time recursive optimization and directly computes control actions based on the current state, whereas OS-SLS-MPC performs a single initial and non-real-time optimization of the nominal trajectory and correction policy, and thus robustly achieves the full constrained rendezvous manoeuvre with a single linear control policy.

5.2 Scenario 2 – Larger Disturbances

The second scenario is the same as the first in every way except for an increase of the maximum disturbance acceleration by 50% to $\gamma_w = 1.5 \mu m/s^2$. In this case, the LTB-MPC optimization problem is always infeasible, but a solution exists for the SLS-MPC formulation. This is due to the fact that SLS-MPC optimizes the ancillary controller and can shape and size of the state and control tubes/reachable sets, whereas it is fixed for LTB-MPC, such that it can only offset but not shape the tubes. We also report that we were not able to recover feasibility after some hand-tuning efforts for the matrices Q, R, and Q_f of

	ΔV [m/s]					
	Scenario 1			Scenario 2		
	Nominal	Mean	Max	Nominal	Mean	Max
LTB-MPC	0.141	0.145	0.156	Infeasible		
SLS-MPC	0.129	0.134	0.149	0.146	0.154	0.173
OS-SLS-MPC	0.143	0.153	0.162	0.166	0.178	0.195

Table 2 Total ΔV performance for each controller for the Monte-Carlo simulations.

the LQR ancillary controller. This result thus further demonstrates the advantages of SLS-MPC, namely in terms of improved feasibility.

The right-hand side of Table 2 also shows the ΔV performance of the SLS-MPC and the OS-SLS-MPC, showing an average increase in the total ΔV of $\approx 16\%$ for the latter, which is due to the fact that for OS-SLS-MPC the nominal trajectory and correction policies are fixed after being initially computed.

Figure 9 compares the ROE trajectories for both controllers, showing that their nominal trajectories are relatively similar. However, OS-SLS-MPC yields tighter dispersions, given that it must perform the full robust constrained manoeuvre with a single linear correction policy that is not updated midway. On the other hand, SLS-MPC uses updated state knowledge during the manoeuvre execution, which allows it to subsequently relax the state and control tubes as much as necessary to minimize the predicted ΔV use, while still ensuring robust constraint satisfaction. On the other hand, as discussed before, OS-SLS-MPC does not rely on real-time recursive optimization, given that the initial and only optimization can be performed while maintaining a time-flexible and safe hold point.

6 Conclusion and Future Work

We addressed the rendezvous guidance and control problem with Robust Model Predictive Control (MPC), namely System Level Synthesis MPC (SLS-MPC). We considered a relative orbital element (ROE) representation of the relative state between the two satellites, which yields an accurate prediction model that includes J_2 and drag perturbations. The ROE state also enables a simple safety concept which was used to derive an approximate polyhedral and convex passive safety constraint, that was shown in a numerical example to have low conservativeness.

We demonstrated the advantages of SLS-MPC with respect to a common practical Robust MPC approach, namely Linear Tube-Based MPC (LTB-MPC). Indeed, the SLS-MPC problem is feasible in a larger range of conditions, given that it optimizes the ancillary controller, i.e., the size and shape of the tubes, together with the nominal trajectory, whereas for LTB-MPC these properties are rigid and thus might yield an infeasible problem if the constraints are tight or/and the disturbances large. Furthermore, SLS-MPC was also shown to yield better closed-loop performance in terms of the objective metric, namely fuel/ΔV, given that this tube flexibility also enables optimizing the fuel consumption for disturbance correction, via the proposed approximate robust objective function.

On the other hand, SLS-MPC is disadvantaged by a computation time two orders of magnitude greater than that of LTB-MPC, a gap that further widens with the problem dimensions. Therefore, SLS-MPC further worsens one of the greatest downsides of MPC, i.e., its significant computational demand. In response to this, we proposed One-Shot SLS-MPC (OS-SLS-MPC), whereby only one SLS optimization is performed, and the resulting nominal trajectory and correction policy are used to robustly execute and complete the full manoeuvre. This strategy was shown to have an increased fuel consumption of 6% with respect to LTB-MPC, but has the advantage of not relying on real-time and recursive numerical

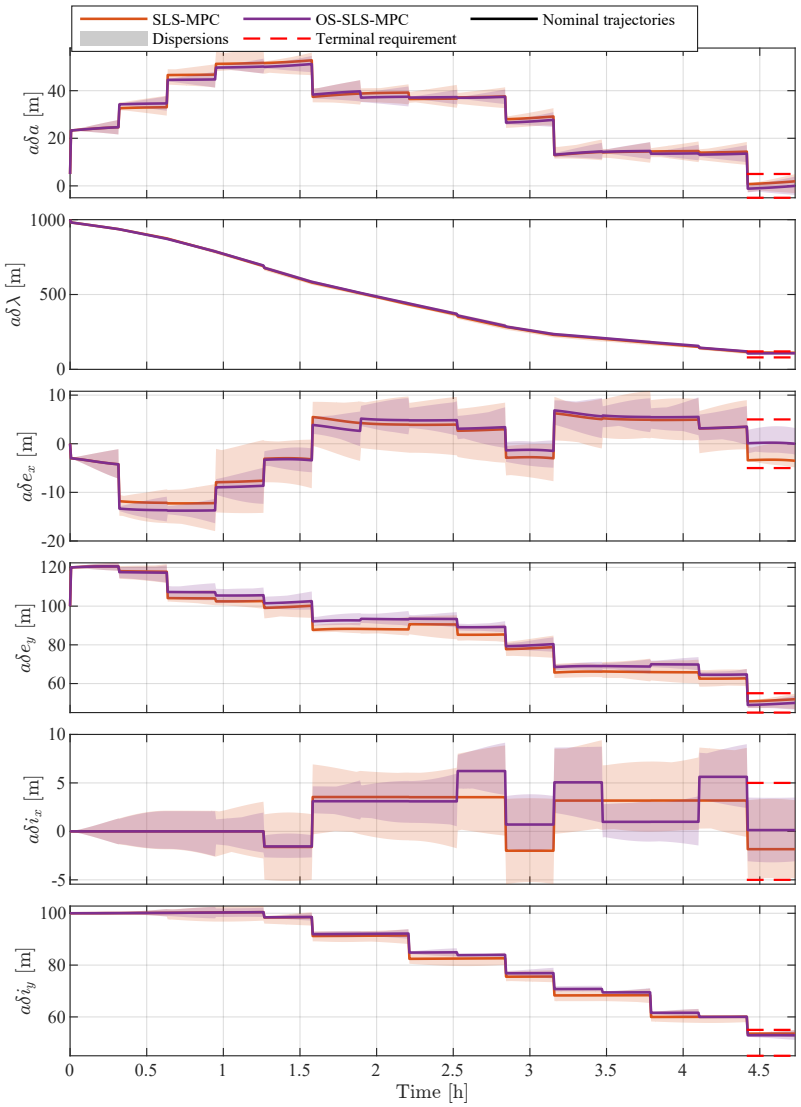

Fig. 9 Time-evolution of the ROE trajectories for full closed-loop SLS-MPC and One-Shot SLS-MPC in Monte-Carlo simulation.

optimization, as well as improved feasibility. It does, however, rely on one computationally heavy initial optimization; but, for a rendezvous application, this optimization can be performed prior to the start of the manoeuvre while maintaining a safe and potentially time-flexible hold point, and thus with softer real-time computation constraints.

Future work shall focus on extending the results to two of the most important sources of uncertainty existing in a rendezvous mission that are currently missing: state estimation errors and execution errors. Furthermore, the proposed approach should be validated with proper model-in-the-loop testing in a high-fidelity simulator. Finally, given the high computational demand of SLS, the formulation of efficient and robust problem-specific optimization solvers should be addressed, to improve the computational tractability of SLS-MPC and even OS-SLS-MPC.

Acknowledgments

This work was supported by national funds through Fundação para a Ciência e a Tecnologia, I.P. (FCT) under projects UID/50021/2025 (DOI: https://doi.org/10.54499/UID/50021/2025) and UID/PRR/50021/2025 (DOI: https://doi.org/10.54499/UID/PRR/50021/2025. The work of Afonso Botelho was supported by the Ph.D. Fellowship by the Portuguese Space Agency— Portugal Space through FCT, Portugal, under Grant PRT/BD/152809/2021 (DOI: https://doi.org/10.54499/PRT/BD/152809/2021).

Declaration of Use of Artificial Intelligence

Artificial intelligence was used to proofread this paper.

References

[1] James B Rawlings, David Q Mayne, and Moritz M Diehl. *Model Predictive Control: Theory, Computation, and Design 2nd Edition*. Nob Hill Publishing, 2 edition, 2017. ISBN: 978-0-9759377-5-4.

[2] Arthur Richards and Jonathan How. Performance evaluation of rendezvous using model predictive control. In *AIAA Guidance, Navigation, and Control Conference and Exhibit*, 2003. doi: 10.2514/6.2003-5507.

[3] Arthur Richards and Jonathan P. How. Robust variable horizon model predictive control for vehicle maneuvering. *International Journal of Robust and Nonlinear Control*, 16(7):333–351, May 2006. ISSN: 1049-8923, 1099-1239. doi: 10.1002/rnc.1059.

[4] Francisco Gavilan, Rafael Vazquez, and Eduardo F. Camacho. Chance-constrained model predictive control for spacecraft rendezvous with disturbance estimation. *Control Engineering Practice*, 20(2):111–122, Feb. 2012. ISSN: 09670661. doi: 10.1016/j.conengprac.2011.09.006.

[5] Edward N. Hartley, Marco Gallieri, and Jan M. Maciejowski. Terminal spacecraft rendezvous and capture with LASSO model predictive control. *International Journal of Control*, 86(11):2104–2113, Nov. 2013. ISSN: 0020-7179, 1366-5820. doi: 10.1080/00207179.2013.789608.

[6] Georgia Deaconu, Christophe Louembet, and Alain Théron. Minimizing the Effects of Navigation Uncertainties on the Spacecraft Rendezvous Precision. *Journal of Guidance, Control, and Dynamics*, 37(2):695–700, Mar. 2014. ISSN: 0731-5090, 1533-3884. doi: 10.2514/1.62219.

[7] Edward N Hartley. A Tutorial on Model Predictive Control for Spacecraft Rendezvous. In *2015 European Control Conference (ECC)*, pages 1355–1361. IEEE, Aug. 2015.

[8] Afonso Botelho, Baltazar Parreira, Paulo N. Rosa, and João Miranda Lemos. *Predictive Control for Spacecraft Rendezvous*. SpringerBriefs in Applied Sciences and Technology. Springer International Publishing, 2021. ISBN: 978-3-030-75695-6. ISSN: 2191-530X, 2191-5318. doi: 10.1007/978-3-030-75696-3.

[9] Per Bodin, Ron Noteborn, Robin Larsson, and Camille Chasset. System test results from the GNC experiments on the PRISMA in-orbit test bed. *Acta Astronautica*, 68(7-8), 2011. ISSN: 00945765. doi: 10.1016/j.actaastro.2010.08.021.

[10] Wigbert Fehse. *Automated Rendezvous and Docking of Spacecraft*. Cambridge University Press, 2003.

[11] NASA. Commercial space. `https://www.nasa.gov/humans-in-space/commercial-space/`. Accessed: 2024-04-29.

[12] James Anderson, John C. Doyle, Steven H. Low, and Nikolai Matni. System level synthesis. *Annual Reviews in Control*, 47:364–393, Jan. 2019. ISSN: 13675788. Publisher: Elsevier Ltd. doi: 10.1016/j.arcontrol.2019.03.006.

[13] Yang Zheng, Luca Furieri, Antonis Papachristodoulou, Na Li, and Maryam Kamgarpour. On the Equivalence of Youla, System-level and Input-output Parameterizations. *IEEE Transactions on Automatic Control*, 66(1):413–420, Jan. 2021. ISSN: 0018-9286, 1558-2523, 2334-3303. doi: 10.1109/TAC.2020.2979785.

[14] D. Youla, H. Jabr, and J. Bongiorno. Modern Wiener-Hopf design of optimal controllers–Part II: The multivariable case. *IEEE Transactions on Automatic Control*, 21(3):319–338, June 1976. ISSN: 0018-9286. doi: 10.1109/TAC.1976.1101223.

[15] Shaoru Chen, Han Wang, Manfred Morari, Victor M. Preciado, and Nikolai Matni. Robust Closed-loop Model Predictive Control via System Level Synthesis. In *2020 59th IEEE Conference on Decision and Control (CDC)*, pages 2152–2159, Dec. 2020. ISSN: 2576-2370. doi: 10.1109/CDC42340.2020.9304200, `https://ieeexplore.ieee.org/abstract/document/9304200`.

[16] Jerome Sieber, Andrea Zanelli, Samir Bennani, and Melanie N. Zeilinger. System level disturbance reachable sets and their application to tube-based MPC. *European Journal of Control*, 68, Nov. 2022. ISSN: 09473580. Publisher: Elsevier Ltd. doi: 10.1016/j.ejcon.2022.100680.

[17] Shaoru Chen, Victor M. Preciado, Manfred Morari, and Nikolai Matni. Robust model predictive control with polytopic model uncertainty through System Level Synthesis. *Automatica*, 162, Apr. 2024. ISSN: 00051098. Publisher: Elsevier Ltd. doi: 10.1016/j.automatica.2023.111431.

[18] Antoine P. Leeman, Jérôme Sieber, Samir Bennani, and Melanie N. Zeilinger. Robust Optimal Control for Nonlinear Systems with Parametric Uncertainties via System Level Synthesis. In *Proceedings of the IEEE Conference on Decision and Control*, pages 4784–4791. Institute of Electrical and Electronics Engineers Inc., 2023. ISBN: 9798350301243. ISSN: 25762370. doi: 10.1109/CDC49753.2023.10383271.

[19] Marcell Bartos, Alexandre Didier, Jerome Sieber, Johannes Köhler, and Melanie N. Zeilinger. Stochastic MPC with Online-optimized Policies and Closed-loop Guarantees, Feb. 2025. doi: 10.48550/arXiv.2502.06469, `http://arxiv.org/abs/2502.06469`.

[20] Antoine P. Leeman, Johannes Kohler, Florian Messerer, Amon Lahr, Moritz Diehl, and Melanie N. Zeilinger. Fast System Level Synthesis: Robust Model Predictive Control using Riccati Recursions. *IFAC-PapersOnLine*, 58(18):173–180, 2024. ISSN: 24058963. doi: 10.1016/j.ifacol.2024.09.027.

[21] Paul J. Goulart, Eric C. Kerrigan, and Jan M. Maciejowski. Optimization over state feedback policies for robust control with constraints. *Automatica*, 42(4):523–533, Apr. 2006. ISSN: 00051098. doi: 10.1016/j.automatica.2005.08.023.

[22] Paul J. Goulart, Eric C. Kerrigan, and Daniel Ralph. Efficient robust optimization for robust control with constraints. *Mathematical Programming*, 114(1):115–147, July 2008. ISSN: 0025-5610, 1436-4646. doi: 10.1007/s10107-007-0096-6.

[23] Mingfei Ye and Ilya Kolmanovsky. Approximating optimal control by shrinking horizon model predictive control for spacecraft rendezvous and docking. *IFAC-PapersOnLine*, 55(16):284–289, 2022. ISSN: 24058963. doi: 10.1016/j.ifacol.2022.09.038.

[24] Miguel Castroviejo-Fernandez, Michele Ambrosino, and Ilya Kolmanovsky. Robust Parametric Shrinking Horizon Model Predictive Control and its Application to Spacecraft Rendezvous. *IEEE Control Systems Letters*, 8:2781–2786, 2024. ISSN: 2475-1456. doi: 10.1109/LCSYS.2024.3514975.

[25] Simone D'Amico. *Autonomous Formation Flying in Low Earth Orbit*. PhD thesis, Politecnico di Milano, 2010.

[26] W. H. Clohessy and R. S. Wiltshire. Terminal Guidance System for Satellite Rendezvous. *Journal of the Aerospace Sciences*, 27(9):653–658, Sept. 1960. Publisher: American Institute of Aeronautics and Astronautics (AIAA). doi: 10.2514/8.8704.

[27] Koji Yamanaka and Finn Ankersen. New state transition matrix for relative motion on an arbitrary elliptical orbit. *Journal of Guidance, Control, and Dynamics*, 25(1):60–66, 2002. ISSN: 07315090. doi: 10.2514/2.4875.

[28] Adam W. Koenig, Tommaso Guffanti, and Simone D'Amico. New state transition matrices for spacecraft relative motion in perturbed orbits. *Journal of Guidance, Control, and Dynamics*, 40(7):1749–1768, 2017. ISSN: 15333884. Publisher: American Institute of Aeronautics and Astronautics Inc. doi: 10.2514/1.G002409.

[29] G. Gaias and J. S. Ardaens. Design challenges and safety concept for the AVANTI experiment. *Acta Astronautica*, 123:409–419, June 2016. ISSN: 00945765. Publisher: Elsevier Ltd. doi: 10.1016/j.actaastro.2015.12.034.

[30] Finn. Ankersen. *Guidance, navigation, control and relative dynamics for spacecraft proximity maneuvers*. PhD thesis, Aalborg University, 2010. ISBN: 9788792328724.

[31] David A. Vallado. *Fundamentals of Astrodynamics and Applications*. Space Technology Library, 2013.

[32] Gabriella Gaias, Camilla Colombo, and Martin Lara. Analytical framework for precise relative motion in low earth orbits. *Journal of Guidance, Control, and Dynamics*, 43(5):915–927, 2020. ISSN: 15333884. Publisher: American Institute of Aeronautics and Astronautics Inc. doi: 10.2514/1.G004716.

[33] Michelle Chernick and Simone D'amico. New Closed-Form Solutions for Optimal Impulsive Control of Spacecraft Relative Motion. *Journal of Guidance, Control, and Dynamics*, 41(2):301–319, Feb. 2018.

[34] Arthur Richards, Tom Schouwenaars, Jonathan P How, and Eric Feron. Spacecraft Trajectory Planning with Avoidance Constraints Using Mixed-Integer Linear Programming. *Journal of Guidance, Control and Dynamics*, 25(4):755–764, 2002.

[35] Louis Breger and Jonathan P How. Safe Trajectories for Autonomous Rendezvous of Spacecraft. *Journal of Guidance, Control, and Dynamics*, 31(5):1478–1489, Sept. 2008.

[36] Hyeongjun Park, Stefano Di Cairano, and Ilya Kolmanovsky. Model predictive control for spacecraft rendezvous and docking with a rotating/tumbling platform and for debris avoidance. In *Proceedings of the American Control Conference*, 2011. ISSN: 07431619. doi: 10.1109/acc.2011.5991151.

[37] Qi Li, Jianping Yuan, Bo Zhang, and Chen Gao. Model predictive control for autonomous rendezvous and docking with a tumbling target. *Aerospace Science and Technology*, 69:700–711, Oct. 2017. ISSN: 12709638. Publisher: Elsevier Masson s.r.l. doi: 10.1016/j.ast.2017.07.022.

[38] Georgia Deaconu, Christophe Louembet, and Alain Théron. Designing Continuously Constrained Spacecraft Relative Trajectories for Proximity Operations. *Journal of Guidance, Control, and Dynamics*, 38(7), 2015. ISSN: 15333884. doi: 10.2514/1.G000283.

[39] Stephen P. Boyd and Lieven. Vandenberghe. *Convex optimization*. Cambridge University Press, 2004. ISBN: 0-521-83378-7.